New insights into the Cs-Mo-O system: Experimental studies of the Cs2MoO4-MoO3 pseudo-binary system

A.L. Smith, J. Vlieland, M.-C. Pignié, M. Abbink, G. Mikaelian, P. Benigni

▶ **To cite this version:**

HAL Id: hal-03117343
https://hal.science/hal-03117343

Submitted on 8 Mar 2022

New insights into the Cs-Mo-O system: experimental studies of the Cs_2MoO_4-MoO_3 pseudo-binary system

A.L. Smith[a,*], J. Vlieland[a], M.-C. Pignié[b], M. Abbink[a], G. Mikaelian[c], P. Benigni[c]

[a]*Delft University of Technology, Faculty of Applied Sciences, Radiation Science & Technology Department, Mekelweg 15, 2629 JB Delft, The Netherlands*
[b]*PSL Research University, Chimie ParisTech-CNRS, Institut de Recherche de Chimie Paris, 75005 Paris, France*
[c]*Aix Marseille University, Université de Toulon, CNRS, IM2NP, Marseille, France*

Abstract

The ternary cesium molybdates $Cs_2Mo_2O_7$, $Cs_2Mo_3O_{10}$, $Cs_2Mo_5O_{16}$ and $Cs_2Mo_7O_{22}$ have been synthesized in this work using a solid state route and their structures have been characterized using X-ray diffraction. The enthalpies of formation of $Cs_2Mo_2O_7$ and $Cs_2Mo_3O_{10}$ have been measured using solution calorimetry, yielding $\Delta_f H_m^o(Cs_2Mo_2O_7, cr, 298.15\ K) = -(2301.6 \pm 4.7)$ kJ·mol^{-1} and $\Delta_f H_m^o(Cs_2Mo_3O_{10}, cr, 298.15\ K) = -(3075.6 \pm 6.5)$ kJ·mol^{-1}, respectively. In addition, the transition temperatures and transition enthalpies of $Cs_2Mo_2O_7$, $Cs_2Mo_3O_{10}$, $Cs_2Mo_5O_{16}$ and $Cs_2Mo_7O_{22}$ have been determined using differential scanning calorimetry. Finally, phase diagram equilibria measurements in the Cs_2MoO_4-MoO_3 pseudo-binary section have been performed, that have yielded generally slightly lower transition temperatures than reported in previous studies. Those data can serve as valuable input for thermodynamic modelling purposes of the fission products chemistry in Light Water Reactors and next generation Sodium-cooled Fast Reactors and Lead-cooled Fast Reactors.

Keywords: Solution calorimetry, Differential Scanning Calorimetry, cesium polymolybdates, Joint Oxyde-Gaine

1. Introduction

The Cs-Mo-O system plays a key role in the fission products chemistry of irradiated fuel in the current generation of Light Water Reactors but also of next generation (Generation IV) solid fueled fast reactors such as the Sodium-cooled Fast Reactors (SFRs) and Lead-cooled Fast reactors (LFRs). Cesium and molybdenum are generated with a high fission yield and are subject of primary

---

*Corresponding author

*Email address:* a.l.smith@tudelft.nl (A.L. Smith)

concern for the public in a severe accident (SA) scenario. Cesium belongs to the so-called volatile fission products [1], while the Mo/MoO_2 redox couple plays a key role in SA analysis as it is believed to act as an oxygen buffer, which determines the chemical state of other fission products (e.g. Cs, Ba, Sr) and their release behaviour [2, 3]. The chemistry of molybdenum is moreover particularly intricate as it can form metallic precipitates or oxide phases (e.g. Mo, MoO_2, Cs_2MoO_4) depending on the burn-up, temperature and oxygen potential of the fuel [4].

The formation of cesium molybdate and polymolybdate phases is particularly relevant for the safety assessment of fast neutron spectrum reactors as the fuel will reach higher burnup (up to 20% FIMA -fission per initial metal atom-), thus higher oxygen potentials in such type of reactors. During irradiation of a $(U,Pu)O_2$ fueled SFR or LFR, the volatile fission products (Cs, Mo, Te, I) migrate from the inner pellet towards the rim due to the very high temperature gradient ($\sim$ 450 K·mm^{-1} with $\sim$ 2273 K in the pellet center and $\sim$ 973 K at the rim), and accumulate above $\sim$ 7-8% FIMA in the space between fuel and cladding in the form of a 150-300 μm layer called the JOG (*Joint Oxyde-Gaine*, a french term to indicate the oxide-cladding joint). Post-irradiation examinations of fuel pins irradiated in the Phénix reactor (France), the Fast Flux Test Facility (FFTF, United States), and the JOYO reactor (Japan), using techniques such as Scanning Electron Microscopy (SEM), Energy Dispersive X-ray Spectroscopy (EDS), Transmission Electron Microscopy (TEM), and Electron Probe Micro Analyses (EPMA) coupled with thermodynamic calculations have suggested that the main constituents of the JOG layer were Cs_2MoO_4 (major phase), CsI, Cs_2Te and Cs_2UO_4 [5–11]. In particular, the recent post-irradiation examinations of an annular $U_{0.71}Pu_{0.29}O_{1.95}$ mixed oxide fuel irradiated in the Fast Flux Test Facility (FFTF) between 1985 and 1992 at a burnup level of 19% FIMA using SEM, EDS and TEM have revealed detailed insights into the morphological, chemical and structural characterization of the JOG [11]. The JOG was reported to have a highly heterogeneous porous structure with inclusions of fission products (Cs, Mo, Te, I, Zr, Ba) and cladding components (Fe, Cr). From Selected Area Electron Data (SAED) obtained by TEM combined with a combinatorial structural analysis using deep learning predictions, the presence of orthorhombic Cs_2MoO_4 was confirmed as the major phase, and the existence of higher order polymolybdates was suggested as well as Fe-Pd alloy with tetragonal structure. Interestingly, the signature of a structure of monoclinic symmetry in space group $C2/m$ was suggested for the first time in localized areas, that was assigned to $Cs_2Mo_3O_{10}$ (monoclinic $C2/c$). The $P2_1/c$ symmetry was also predicted in other localized areas, that was attributed to $Cs_2Ba_2O_3$ (following Cs decay into Ba), but could in fact correspond to α-$Cs_2Mo_2O_7$, itself monoclinic in space group $P2_1/c$.

The structural, thermodynamic, and thermo-physical properties (e.g. thermal expansion, thermal conductivity) of the components of the JOG, including the cesium molybdate and polymolybdate phases, are of importance as input data for the modelling of the JOG in Fuel Performance Codes. It is also of interest for the modelling of the fission product release under accidental conditions

and of the corrosion of the steel cladding by the fission products.

The main component of the JOG, i.e. Cs_2MoO_4, shows a phase transition at (841.3 ± 1.0) K from an orthorhombic phase (α-form, in space group $Pnma$) to a hexagonal phase (β-form in space group $P6_3/mmc$) [12, 13]. The thermal conductivity of Cs_2MoO_4 measured up to the melting point $T_{fus} = (1229.5 \pm 0.2)$ K [12] was reported to be one order of magnitude lower than the fuel [14, 15], which could lead to the creation of hot spots and modify the radial temperature distribution in the fuel pellet. The thermal expansion of orthorhombic α-Cs_2MoO_4 was found to be high and to increase substantially with temperature, which means swelling in the gap between fuel and cladding could be significant. Besides, the expansion of hexagonal β-Cs_2MoO_4 was found to be strongly anisotropic (α_c-$\alpha_a = 67\ 10^{-6}$ K^{-1}), which is detrimental to its mechanical properties and leads to a risk of cracking [13]. Finally vapour pressure studies [16] have suggested a decomposition to $Cs_2Mo_2O_7$ and $Cs(g)$ and $O_2(g)$ at high temperatures, according to the following equilibrium reaction:

$$2Cs_2MoO_4(cr) = Cs_2Mo_2O_7(cr) + 2Cs(g) + \frac{1}{2}O_2(g) \qquad (1)$$
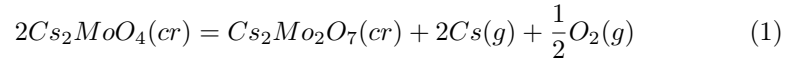
The formation of $Cs(g)$ at the periphery of the fuel is of concern as a possible release of ^{135}Cs and ^{137}Cs into the coolant could take place in case of a clad breach. To assess the driving force for the release of radioactive materials (source term) in accidental conditions, a comprehensive knowledge of the thermodynamic properties of the JOG phases is thus of paramount importance.

One main challenge for the fuel community is that the exact chemical composition of the JOG as a function of burnup, temperature and oxygen potential is still largely unknown, and the mechanisms of its formation are still not well understood. In this context, this work aims to obtain reliable experimental data for the Cs-Mo-O system, a key sub-system of the JOG multi-element system (Cs-Mo-I-Te-U-Zr-Ba-Fe-Cr-O), which can serve as input for the development of reliable thermodynamic models based on the CALPHAD (CALculation of PHAse Diagram) methodology.

2. Brief review of literature data

The Cs-Mo-O system is rather complex, with many ternary phases reported, i.e. hexavalent molybdates Cs_2MoO_4, $Cs_2Mo_2O_7$, $Cs_2Mo_3O_{10}$, $Cs_2Mo_4O_{13}$, $Cs_2Mo_5O_{16}$ and $Cs_2Mo_7O_{22}$, $Cs_6Mo_2O_9$, but also mixed valence states (so-called bronze) compounds $Cs_{0.14}MoO_3$, $Cs_{0.25}MoO_3$, $Cs_{0.3}MoO_3$, $Cs_{0.33}MoO_3$ and $CsMo_{4-x}O_{12}$ [17, 18]. A comprehensive review of the literature data available on the Cs-Mo-O system has been reported by Fabrichnaya [17] and a critical evaluation of available thermodynamic data has been performed by Cordfunke and Konings [19].

Only a limited number of experimental studies of the thermodynamic properties have been reported to this date, mainly focusing on Cs_2MoO_4 and $Cs_2Mo_2O_7$, the phases expected under reactor conditions [12, 16, 19–25]. The standard

3

enthalpies of formation of both compounds have been measured by solution calorimetry by O'Hare and Hoekstra [20, 23]. The result for Cs_2MoO_4 was recently confirmed by Smith et al. [26] using a similar method. The standard entropies have been derived from low-temperature heat capacity measurements using adiabatic calorimetry for Cs_2MoO_4 [22] and thermal-relaxation calorimetry for $Cs_2Mo_2O_7$ [21]. High temperature enthalpy increment measurements have been reported for Cs_2MoO_4 by Fredrickson and Chasanov [27] (845-1191 K), Konings and Cordfunke [12] (415-700 K), and Denielou et al. [28] (1232-1500 K). The data of Fredrickson and Chasanov show discrepancies with the other sets of data, and were discarded in the review of Cordfunke and Konings, however [19]. In addition, Kohli and Lacom [29] performed direct heat capacity measurements in the range 300 to 800 K using differential scanning calorimetry (DSC). The phase transition and melting temperatures of Cs_2MoO_4 were determined by Hoekstra [30], Konings and Cordfunke [12], Denielou et al. [28], and Smith et al. [21]. The enthalpy associated with the α to β phase transition in Cs_2MoO_4 was measured by Konings and Cordfunke [12] and Fredrickson and Chasanov [27] by DSC, with a very good agreement between the two studies. Finally, the melting enthalpy of β-Cs_2MoO_4 was obtained by Denielou et al. [28] from drop calorimetry data. The high temperature heat capacity of $Cs_2Mo_2O_7$ has been reported in the range 310 to 700 K by Kohli [24] based on DSC measurements, but found in poor agreement with the low-temperature heat capacity data of Smith et al. [21]. Finally, the phase transition and melting temperatures of $Cs_2Mo_2O_7$ have been measured by Hoekstra [30] and Smith et al. [21]. The corresponding transition enthalpies have not been determined to this date.

Spitsyn and Kuleshov [31], Salmon and Caillet [32], Hoekstra [30] and Bazarova et al. [33] investigated the Cs_2MoO_4-MoO_3 phase diagram using thermal analysis by a visual-polythermal technique (Spitsyn and Kuleshov) [31], solid state reactions coupled with X-ray diffraction (XRD), Differential Thermal Analysis (DTA) and infrared spectroscopy (Salmon and Caillet), a combination of X-ray diffraction analyses, simultaneous DTA-TGA (Differential Thermal Analysis-Thermogravimetry Analysis) measurements, infrared and Raman spectroscopy studies (Hoekstra) [30], and a combination of XRD, DTA, infrared spectroscopy and electric conductivity measurements (Bazarova et al.), respectively. The measured equilibrium data [30, 31] in the Cs_2MoO_4-MoO_3 pseudo-binary section are shown in Figure 2. A number of discrepancies can be noticed between the various studies. The results of Hoekstra are believed to be most reliable as reported in the review of Fabrichnaya [17].

More recently, a thermodynamic model of this system has been developed as part of the TAF-ID database [34] based on the available thermodynamic and phase diagram data. The phase equilibria as reported by Hoekstra [30] were selected for the assessment, and a good agreement with those data is generally observed. The polymorphic transition of $Cs_2Mo_2O_7$ was not included in the model. A subsequent study of the $Cs_2Mo_2O_7$ compound by Smith et al. [21] has highlighted some discrepancies with previous data and the model, however [21]. The goal of the present study is to provide further thermodynamic data

4

on the higher polymolybdates to help solve discrepancies on this system and serve as input for modelling purposes. The standard enthalpy of formation of $Cs_2Mo_2O_7$ at 298.15 K was measured to validate the data of O'Hare and Hoekstra [23], and that of $Cs_2Mo_3O_{10}$ was obtained for the first time. Phase diagram measurements were performed in the Cs_2MoO_4-MoO_3 pseudo-binary section, and the transition enthalpies of $Cs_2Mo_2O_7$, $Cs_2Mo_3O_{10}$, $Cs_2Mo_5O_{16}$ and $Cs_2Mo_7O_{22}$ were determined.

3. Experimental methods

3.1. Sample preparation

The cesium polymolybdates were synthesized by reaction between accurately weighted quantities of cesium orthomolybdate Cs_2MoO_4 and molybdenum oxide (MoO_3, 99.95%, Sigma-Aldrich). The cesium orthomolybdate starting material was synthesized as described in [13] by reaction between stoichiometric amounts of cesium carbonate (Cs_2CO_3, 99.99 %, Alfa Aesar) and molybdenum oxide. Two batches of $Cs_2Mo_2O_7$ were prepared. The first one, used for the solution calorimetry measurements, was synthesized as described in [21]. The second one, used for the Differential Scanning Calorimetry (DSC) measurements, and subsequent synthesis of $Cs_2Mo_3O_{10}$, was made with a (Cs_2MoO_4:MoO_3) stoichiometric mixture heated in a platinum crucible under oxygen flow at 823 K for 16 h, followed by regrinding and thermal treatment at 623 K for 16 h. $Cs_2Mo_3O_{10}$ was then prepared with a stoichiometric mixture of ($Cs_2Mo_2O_7$:MoO_3) heated under oxygen flow in a platinum crucible at 923 K for 16 h, followed by a slow cooling down to room temperature (1 K·min^{-1}).

$Cs_2Mo_3O_{10}$, $Cs_2Mo_5O_{16}$ and $Cs_2Mo_7O_{22}$ materials were also synthesized as described in detail by Benigni et al. [35] by reaction between stoichiometric amounts of cesium orthomolybdate (Cs_2MoO_4, 99.9%, Alfa Aesar) and molybdenum oxide (MoO_3, 99.95%, Alfa Aesar) in a platinum crucible heated under air until a liquid phase or complete melting occurred.

The purity of the samples was examined by X-ray diffraction (XRD) at room temperature and Differential Scanning Calorimetry (DSC). No secondary phases were detected by XRD. Moreover, no additional peak was detected in the DSC measurements that could be attributed to impurities for the Cs_2MoO_4, $Cs_2Mo_2O_7$ and $Cs_2Mo_3O_{10}$ materials, and the corresponding purities were estimated to be 99%, 99% and 98.5%, respectively. One additional thermal event with small magnitude was detected in the $Cs_2Mo_5O_{16}$ and $Cs_2Mo_7O_{22}$ materials as reported in detail in section 4.4. These were attributed to the peritectoid decomposition of $Cs_2Mo_4O_{13}$, and peritectic decomposition of $Cs_2Mo_5O_{16}$ impurities, respectively. The purities of those two materials were thus estimated at 97% (see Table 1).

For the transition enthalpy determinations, the use of reference materials was also necessary. Na_2MoO_4 (anhydrous, 99.9%, Sigma-Aldrich) and Cs_2TeO_4 synthesized by reaction between tellurium oxide TeO_2 (99.995%, Alfa Aesar) and cesium carbonate Cs_2CO_3 (99.99 %, Sigma-Aldrich) as described in detail in [36] were used.

Table 1: Provenance and purity of the samples used in this study. XRD: X-ray diffraction; DSC: Differential Scanning Calorimetry.

Formula	Source	State	Color	Mass fraction purity[a]	Purity analysis method
MoO_3	Sigma-Aldrich/Alfa Aesar	Powder	Light green	0.9995 ± 0.0005	Provided by supplier
Cs_2CO_3	Alfa Aesar	Powder	White	0.9999 ± 0.0001	Provided by supplier
Cs_2MoO_4	Alfa Aesar	Powder	White	0.999 ± 0.001	Provided by supplier
Cs_2MoO_4	Synthesized	Powder	White	0.99 ± 0.01	XRD, DSC
$Cs_2Mo_2O_7$	Synthesized	Powder	White	0.99 ± 0.01	XRD, DSC
$Cs_2Mo_3O_{10}$	Synthesized	Powder	White	0.985 ± 0.015	XRD, DSC
$Cs_2Mo_5O_{16}$	Synthesized	Powder	White	0.97 ± 0.03	XRD, DSC
$Cs_2Mo_7O_{22}$	Synthesized	Powder	White	0.97 ± 0.03	XRD, DSC
TeO_2	Alfa Aesar	Powder	White	0.99995 ± 0.00005	Provided by supplier
Cs_2TeO_4	Synthesized	Powder	Grey	0.99 ± 0.01	XRD, DSC
Na_2MoO_4	Sigma-Aldrich	Powder	White	0.999 ± 0.001	Provided by supplier
CsOH 50% w/w aq. soln	Alfa Aesar	Solution	Transparent	0.999 ± 0.001	Provided by supplier

[a]The quoted uncertainties correspond to standard uncertainties.

3.2. Powder X-ray diffraction (XRD)

The X-ray diffraction patterns were collected at room temperature (295 ± 3^1 K) using a PANalytical X'Pert PRO X-ray diffractometer mounted in the Bragg-Brentano configuration with a Cu anode (0.4 mm x 12 mm line focus, 45 kV, 40 mA). A real time multi strip (RTMS) detector (X'Celerator) was used for the measurement of the X-ray scattered intensities. The data were collected by step scanning in the angle range $10° \leq 2\theta \leq 120°$ with a step size of $0.008°$ (2θ); total measuring time was about 8 h. Structural analysis was performed by the Rietveld method with the Fullprof2k suite [37].

3.3. Solution calorimetry

The enthalpies of dissolution of $Cs_2Mo_2O_7$ and $Cs_2Mo_3O_{10}$ materials were measured using a TA Instruments Precision Solution Calorimeter (semi-adiabatic or isoperibolic calorimeter) and TAM IV thermostat. The calorimetric unit consists of a reaction vessel and stirrer system (motor and gold stirrer holding a glass ampoule). The experiments were performed in a thin-walled 25 mL Pyrex-glass reaction vessel equipped with a thermistor for measuring the temperature rise and a heater for calibration during the measurement and equilibration of the initial baseline in the optimal operating range of the calorimeter before starting the experiment. The samples to be studied were placed inside a 1 mL glass ampoule, which was subsequently sealed using a rubber stopper and bee wax. The latter operation was performed in the dry atmosphere of an argon-filled glove box (H_2O and O_2 content below 5 ppm). The solid samples were dissolved into

---

[1]The quoted uncertainty is a standard uncertainty.

a cesium hydroxide CsOH solution by breaking the bottom of the glass ampoule on the sapphire breaking tip mounted at the bottom of the reaction vessel. The heat of breaking is exothermic, with a value below 10 mJ, and can thus be neglected. The temperature during the measurements was maintained in the oil bath with an accuracy of $\pm$ $1 \cdot 10^{-4}$ K. Electrical calibrations were performed immediately before and after each enthalpy of reaction measurement so as to determine the energy equivalent of the system.

The accuracy of the measurements was verified by measuring the enthalpy of dissolution of potassium chloride (KCl, Sigma-Aldrich, 99.7%) in distilled water. The experimentally determined dissolution enthalpy of KCl(cr) into 1000 H_2O (molality m=0.05551 mol·kg^{-1}), i.e. $\Delta_{diss}H_m^o$(1000H_2O, 298.15 K) = (17.510 $\pm$ 0.024) kJ·mol^{-1} corresponding to $\Delta_{diss}H_m^o$(500H_2O, 298.15 K) = (17.560 $\pm$ 0.024) kJ·mol^{-1} after correction as recommended by the National Bureau of Standards (NBS) [38][2] to m=0.111 mol·kg^{-1}, was found in very good agreement with the value recommended by the NBS [38, 40], i.e. $\Delta_{diss}H_m^o$(500H_2O, 298.15 K) = (17.584 $\pm$ 0.017) kJ·mol^{-1} for the dissolution of KCl(cr) into 500 H_2O (molality m=0.111 mol·kg^{-1}). The measured value corresponds to an enthalpy at infinite dilution of $\Delta_{diss}H_m^o$(∞H_2O, 298.15 K) = (17.217 $\pm$ 0.024) kJ·mol^{-1}, in very good agreement with the NBS data in [38, 40], i.e. $\Delta_{diss}H_m^o$(∞H_2O, 298.15 K) = (17.241 $\pm$ 0.018) kJ·mol^{-1}, and that in [41], i.e. $\Delta_{diss}H_m^o$(∞H_2O, 298.15 K) = 17.22 kJ·mol^{-1}. In addition, the enthalpies of formation of Cs_2MoO_4 and Na_2MoO_4 were determined with this instrument in cesium hydroxyde CsOH and sodium hydroxide NaOH solutions, respectively, as described in a previous work [26], and found in excellent agreement with the literature data [19, 20, 42–44], which gives us good confidence on the reliability of the measurements. The uncertainties on the dissolution enthalpies of MoO_3, $Cs_2Mo_2O_7$ and $Cs_2Mo_3O_{10}$ are reported as expanded uncertainties U with a coverage factor of $k = 2$ (twice the standard deviation of the mean), which corresponds to a confidence interval of ~95% [45].

3.4. Differential Scanning Calorimetry (DSC)

The transition temperatures and transition enthalpies of $Cs_2Mo_2O_7$, $Cs_2Mo_3O_{10}$, $Cs_2Mo_5O_{16}$ and $Cs_2Mo_7O_{22}$ were determined by 3D-heat flux DSC measurements using a Setaram Multi HTC module of the 96 Line calorimeter. Phase diagram measurements in the Cs_2MoO_4-MoO_3 pseudo-binary section were performed using simultaneous Thermogravimetry Analysis (TGA)-Differential Scanning Calorimetry (DSC) measurements using the TGA-DSC module of the same 96 Line calorimeter. In the latter case, the DSC sensors were of plate type.

---

[2]The correction mentioned here was performed as recommended by the NBS in [38]: the measured dissolution enthalpy was corrected to the molality of the certified enthalpy value m=0.111 mol·kg^{-1} using the relationship ΔH^o(500H_2O, 298.15 K)=ΔH(nH_2O, 298.15 K) $- \{\Phi_L(nH_2O) - \Phi_L(500H_2O)\}$, where ΔH(nH_2O, 298.15 K) is the measured dissolution enthalpy corrected to the reference temperature, and the term $\{\Phi_L(nH_2O) - \Phi_L(500H_2O)\}$, derived from Parker's tabulation [39] and listed in [38], corrects the molality to the certified value. The uncertainty on the correction was estimated not to exceed 5 J·mol^{-1} [38].

The temperatures were monitored throughout the experiments by a series of interconnected S-type thermocouples. The temperature on the heating ramp (5 or 10 K·min^{-1} for the measurements) was calibrated and corrected for the effect of the heating rate by measuring the melting points of standard high purity metals (In, Sn, Pb, Al, Ag, Au) at 2-4-6-8-10-12 K·min^{-1}. The calibration procedure was performed as recommended in [46]. The transition temperatures in the Cs_2MoO_4-MoO_3 phase diagram and congruently melting temperatures of Cs_2MoO_4, $Cs_2Mo_2O_7$ and $Cs_2Mo_3O_{10}$ were derived on the heating ramp as the onset temperature using tangential analysis of the recorded heat flow. The liquidus temperature of mixtures was derived from the peak extremum of the last thermal event. An example of the derivation of the different temperatures is shown in the Appendix. The uncertainty on the measured temperatures is estimated to be ± 5 K for pure phases and ± 10 K for mixtures.

The samples were placed in an alumina crucible with boron nitride powder to avoid chemical interactions with the crucible upon melting (which would lead to the formation of aluminium molybdate). It should be noted that with the present measurement configuration (measurements using an alumina crucible and boron nitride protective powder under oxygen flow), the data could be collected up to a maximum temperature of about 1173 K. Above the latter temperature, oxidation of the boron nitride powder was observed which affected the shape of the heat flow baseline curve. Data at higher temperatures could be obtained using gold crucibles as done in the work by Hoekstra [30], or platinum crucibles, but these were reported to slowly react with the melted molybdates [30].

The enthalpies of fusion of $Cs_2Mo_2O_7$ and $Cs_2Mo_3O_{10}$ and peritectic decompositions of $Cs_2Mo_5O_{16}$ and $Cs_2Mo_7O_{22}$ were moreover determined by placing a reference material of well-known transition enthalpy in the reference crucible and measuring both sample and reference materials in the same heating cycle. This configuration allows to calculate for each individual measurement cycle the detector sensitivity equal to:

$$s_{ref} = \frac{M_{ref} \cdot A_{ref}}{m_{ref} \cdot \Delta_{tr}H_{m}^{o}(T_{tr,ref})}$$ (2)

where s_{ref} is the detector sensitivity in μV·mW^{-1}, M_{ref} the molar mass in g·mol^{-1}, m_{ref} the weight of the reference in mg, A_{ref} the peak area corresponding to the transition event in μV·s, and $\Delta_{tr}H_{m}^{o}(T_{tr,ref})$ the enthalpy of transition of the reference material in J·mol^{-1}.

The detector sensitivity is assumed to remain the same at the temperature of the melting event of the sample, which is a reasonable approximation for two events sufficiently close to each other.

4. Results and discussion

4.1. Structural analysis

α-$Cs_2Mo_2O_7$, $Cs_2Mo_3O_{10}$, $Cs_2Mo_5O_{16}$ and $Cs_2Mo_7O_{22}$ crystallize with monoclinic structures, in space groups $P2_1/c$ (14), $C2/c$ (15), $C2/c$ (15), and $C2/c$

(15), respectively. The refined cell parameters obtained by Rietveld and Le Bail methods applied to the collected X-ray diffraction data are summarized in Table 2, and the X-ray diffraction patterns are shown in Figure 1. The refined lattice parameters were found in good agreement with the literature data (α-$Cs_2Mo_2O_7$ [21], $Cs_2Mo_3O_{10}$ [47], $Cs_2Mo_5O_{16}$ [48], $Cs_2Mo_7O_{22}$ [48]).

Table 2: Refined lattice parameters of the cesium polymolybdates. X-ray diffraction measurements were performed at room temperature $T = (295 \pm 3^a)$ K and atmospheric pressure. The derived standard uncertainties are given in parenthesis.

Phase	Symmetry	Space group	a^a/nm	b^a/nm	c^a/nm	$\beta^a/^o$	ρ^a/g·cm^{-3}
α-$Cs_2Mo_2O_7{}^{b,d}$	monoclinic	$P2_1/c$	1.5560 ± 0.0002	1.5184 ± 0.0001	0.72244 ± 0.00007	90.120 ± 0.007	4.4339 ± 0.0007
$Cs_2Mo_3O_{10}{}^{c,d}$	monoclinic	$C2/c$	1.4470 ± 0.0003	0.8402 ± 0.0002	0.9465 ± 0.0002	97.749 ± 0.002	4.157 ± 0.002
$Cs_2Mo_3O_{10}{}^{b,d}$	monoclinic	$C2/c$	1.4472 ± 0.0002	0.8404 ± 0.0001	0.9464 ± 0.0001	97.731 ± 0.006	4.1557 ± 0.0008
$Cs_2Mo_5O_{16}{}^{b,d}$	monoclinic	$C2/c$	2.1444 ± 0.0002	0.55600 ± 0.00004	1.4339 ± 0.0001	122.735 ± 0.005	4.6254 ± 0.0006
$Cs_2Mo_7O_{22}{}^{b,e}$	monoclinic	$C2/c$	2.1546 ± 0.0001	0.55385 ± 0.00003	1.89179 ± 0.00009	122.744 ± 0.003	4.5105 ± 0.0004

^{a}The quoted uncertainty corresponds to the standard uncertainty.

^{b}Batch used for the TG-DSC and DSC measurements.

^{c}Batch used for the solution calorimetry measurements.

^{d}Data obtained from a Rietveld fit.

^{e}Data obtained from a Le Bail fit.

4.2. Determination of the standard enthalpies of formation

4.2.1. α-$Cs_2Mo_2O_7$

The standard enthalpy of formation of α-$Cs_2Mo_2O_7$ was firstly determined in CsOH solution, with a thermochemical cycle very similar to that reported by of O'Hare and Hoekstra for Cs_2MoO_4 [20] and α-$Cs_2Mo_2O_7$ [23], but using a slightly lower concentration of the CsOH solution (0.1002 mol·kg^{-1} instead of $\sim$0.218 mol·kg^{-1} in the work of O'Hare and Hoekstra). Cesium dimolybdate and molybdenum oxide (MoO_3, 99.95%, Alfa Aesar) were dissolved in 0.1002 mol·kg^{-1} and 0.1182 mol·kg^{-1} CsOH solutions, respectively. The reaction scheme used to derive the standard enthalpy of formation is listed in Table 4. The individual calorimetric results for the dissolution of both compounds in successive experiments are listed in Table 3. The dissolutions were in all cases instantaneous.

The weights of dissolved samples were adjusted so that the solutions formed by reactions (1a) and (2a) in Table 4 were identical. One thus obtains the enthalpy of reaction $\Delta_r H_m^o = \Delta_r H_{2a} - \Delta_r H_{1a} = -(121.16 \pm 4.29)$ kJ·mol^{-1} for the following equilibrium:

$$2MoO_3(cr) + 2CsOH(sln) = \alpha - Cs_2Mo_2O_7(cr) + H_2O(sln) \qquad (3)$$
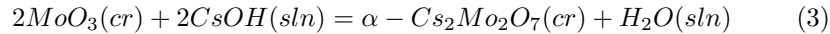
The measured molar dissolution enthalpy of MoO_3(cr) in 25 mL of 0.1182 mol·kg^{-1} CsOH solution, i.e. $\Delta_r H_{2a} = -(75.47 \pm 1.72)$ kJ·mol^{-1}, is in good agreement with previous results by O'Hare and Hoekstra in 99.41 mL of $\sim$0.24

(a) α-$Cs_2Mo_2O_7$

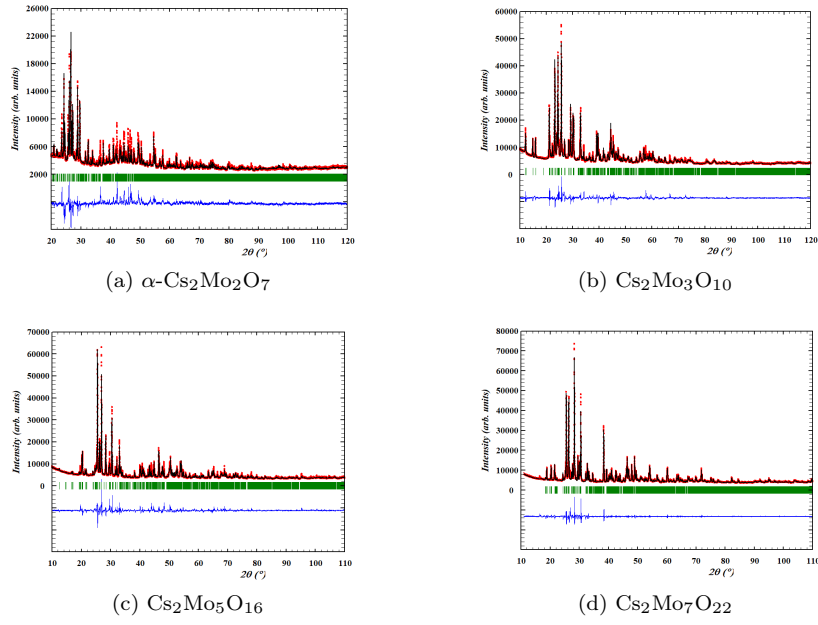(b) $Cs_2Mo_3O_{10}$

(c) $Cs_2Mo_5O_{16}$

(d) $Cs_2Mo_7O_{22}$

Figure 1: Comparison between the observed (Y_{obs}, in red) and calculated (Y_{calc}, in black) X-ray diffraction patterns of (a) α-$Cs_2Mo_2O_7$, (b) $Cs_2Mo_3O_{10}$, (c) $Cs_2Mo_5O_{16}$ and (d) $Cs_2Mo_7O_{22}$. $Y_{obs} - Y_{calc}$, in blue, is the difference between the experimental and calculated intensities. The Bragg reflections' angular positions are marked in green. Measurement at λ=Cu-Kα, with Cu-Kα1, λ = 1.541 Å, Cu-Kα2, λ = 1.544 Å.

Table 3: Calorimetric results for the dissolution of $Cs_2Mo_2O_7$ (M=569.713 g·mol^{-1}) in 0.1002[a] mol·kg^{-1} CsOH solution, and MoO_3 (M=143.947 g·mol^{-1}) in 0.1182[a] mol·kg^{-1} CsOH at 298.15 K. Solution calorimetry measurements were performed in (25.00 ± 0.03[b]) mL solution at a pressure p= (0.105 ± 0.005[b]) MPa, and in the temperature interval T= (298.15 ± 0.30[b]) K

No.	$m(Cs_2Mo_2O_7)^c$/mg	ΔT^d/mK	C_p^e/J·K^{-1}	Q^f/J	$\Delta_r H_m^o$(298.15 K)^g/kJ·mol^{-1}
1	121.5	56.7	113.9	-6.5	-30.3
2	121.5	55.1	113.9	-6.3	-29.4
3	123.5	59.4	113.9	-6.8	-31.2
4	122.0	53.7	112.4	-6.0	-28.2
average					**-29.8 ± 2.6**^{e}
No.	$m(MoO_3)^c$/mg	ΔT^d/mK	C_p^e/J·K^{-1}	Q^f/J	$\Delta_r H_m^o$(298.15 K)^g/kJ·mol^{-1}
1	61.0	275.8	114.6	-31.6	-74.6
2	61.1	284.0	114.0	-32.4	-76.3
3	61.0	282.5	113.3	-32.0	-75.6
average					**-75.5 ± 1.7**^{e}

m is the sample weight, ΔT the temperature change caused by the dissolution, C_p the energy equivalent of the calorimeter, Q the amount of heat generated by the dissolution, $\Delta_r H_m^o$(298.15 K) the corresponding molar enthalpy of reaction. ^{a}The expanded uncertainties (k=2) on the molalities are U = 0.0002 mol·kg^{-1}. ^{b}The quoted uncertainty corresponds to the standard uncertainty. ^{c}The expanded uncertainties (k=2) on the weights are $U(m)$ = 0.1 mg. ^{d}The relative expanded uncertainties (k=2) on ΔT are $U_r(\Delta T)$ = 0.02. ^{e}The relative expanded uncertainties (k=2) on C_p are $U_r(C_p)$ = 0.01. ^{f}The relative expanded uncertainties (k=2) on Q are $U_r(Q)$ = 0.02. ^{g}The expanded relative uncertainties (k=2) on $\Delta_r H_m^o$(298.15 K) are $U_r(\Delta_r H_m^o(298.15K))$ = 0.02. ^{e}Expanded uncertainty (k=2), corresponding to a 95% confidence interval.

mol·kg^{-1} CsOH solution [20], i.e. $-(78.02 \pm 0.13)$ kJ·mol^{-1}, by Smith et al. in 25 mL of 0.1483 mol·kg^{-1} solution [26], i.e. $-(76.47 \pm 0.78)$ kJ·mol^{-1}, and by Benigni et al. in 8 mL of 0.24061 mol·kg^{-1} CsOH solution [35], i.e. $-(77.33 \pm 0.99)$ kJ·mol^{-1}. The enthalpy of reaction (4a) in Table 4 was derived as in a previous publication [26] from the enthalpy of formation of CsOH(aq) reported by Gunn [49], i.e., $\Delta_f H_m^o$(CsOH, aq, 298.15 K) $= -(488.110 \pm 0.042)$ kJ·mol^{-1}, based on the dissolution reaction $Cs(cr) + (n+1)H_2O(l) = CsOH(aq) \cdot nH_2O + 0.5H_2(g)$, and the CODATA value for the enthalpy of formation of $H_2O(l)$, $\Delta_f H_m^o$(H_2O, l, 298.15 K) $= -(285.83 \pm 0.04)$ kJ·mol^{-1} [50]. As stressed in [26], the latter value is consistent with the recommended data for the enthalpy of formation of CsOH(cr) by Gurvich et al. [51] and Konings et al. [52], i.e. $\Delta_f H_m^o$(CsOH, cr, 298.15 K) $= -(416.2 \pm 0.5)$ kJ·mol^{-1} and the measured dissolution enthalpy of CsOH(cr) in H_2O, i.e. $\Delta_{diss} H_\infty^o$(298.15 K) $= -(71.9 \pm 0.4)$ kJ·mol^{-1} [51, 52]. The enthalpy of formation of MoO_3(cr) was taken from the review work by Cordfunke and Konings [19]. Finally, the correction for the relative partial molar enthalpy of water in 0.1002 mol·kg^{-1} CsOH solution was found negligible based on [50, 53].

The summation of reactions (1a)-(6a) such that $\Delta_r H_{7a} = \Delta_r H_{1a} - \Delta_r H_{2a} + 2\Delta_r H_{3a} + \Delta_r H_{4a} + \Delta_r H_{5a} - \Delta_r H_{6a}$ yields the standard enthalpy of formation of α-$Cs_2Mo_2O_7$ as $\Delta_f H_m^o(\alpha$-$Cs_2Mo_2O_7$, cr, 298.15 K) $= -(2301.6 \pm 4.7)$ kJ·mol^{-1}. The

latter value is in very good agreement within uncertainties with that measured by O'Hare and Hoekstra in $\sim$0.218 mol·kg^{-1} CsOH solution (99.41 mL) using a LKB-8700 Precision Calorimeter System [23], which is also the value recommended in the review by Cordfunke and Konings [19] with an increased uncertainty, i.e., $-(2302.4 \pm 2.1)$ kJ·mol^{-1}. It also agrees with the recent measurement by Benigni et al. [35] using a CALSET calorimeter (in-house built Tian-Calvet calorimeter) in 0.21882 mol·kg^{-1} CsOH solution, i.e. $-(2301.84 \pm 2.37)$ kJ·mol^{-1}.

In the present analysis, the uncertainty on the enthalpy of formation of MoO_3(cr) is most probably largely underestimated, however. The value recommended by Cordfunke and Konings [19], i.e. $-(745.0 \pm 1.0)$ kJ·mol^{-1} is taken from the average of the data reported by Staskiewicz et al. [54] $(-744.65 \pm 0.40$ kJ·mol$^{-1})$ and Mah [55] $(-745.4 \pm 0.5$ kJ·mol$^{-1})$. The two values are in excellent agreement. But in both studies, based on the combustion of molybdenum and MoO_2, the oxidation to MoO_3 was incomplete, and although corrections were made for the incomplete combustion (70-93%), the stated final uncertainties (less than 0.07 %) are most probably underestimated. Cordfunke and Konings [19] increased the uncertainty to 0.1%, but it is believed this is still too conservative. Considering that an uncertainty of 1% on the enthalpy of formation of MoO_3(cr) is more realistic (i.e. $\pm$ 7.45 kJ·mol^{-1}), the derived value for the enthalpy of formation of $Cs_2Mo_2O_7$ becomes $-(2301.6 \pm 15.5)$ kJ·mol^{-1}.

Table 4: Thermochemical cycle used for the determination of the enthalpy of formation of α-$Cs_2Mo_2O_7$. Solution calorimetry measurements were performed at a pressure $p= (0.105 \pm 0.005^a)$ MPa, and in the temperature interval $T= (298.15 \pm 0.30^a)$ K. The enthalpy of formation of $Cs_2Mo_2O_7$ is derived with the relation: $\Delta_rH_{7a}=\Delta_rH_{1a}-\Delta_rH_{2a}+2\Delta_rH_{3a}+\Delta_rH_{4a}+\Delta_rH_{5a}-\Delta_rH_{6a}$.

	Reaction	$\Delta_r\mathbf{H_m^o}$(298.15 K)/ kJ·mol^{-1}	Ref.
(1a)	α-$Cs_2Mo_2O_7$(cr) + 11.722($CsOH\cdot555.556H_2O$) = $2Cs_2MoO_4$(sln) + 9.722CsOH(sln) + 6513.227H_2O(sln)	-29.8 ± 2.6^a	This work
(2a)	$2MoO_3$(cr) + 13.722($CsOH\cdot474.510H_2O$) = $2Cs_2MoO_4$(sln) + 9.722CsOH(sln) + 6513.227H_2O(sln)	-151.0 ± 3.4^a	This work
(3a)	Mo(cr) + 3/2O_2(g) = MoO_3(cr)	-745.0 ± 1.0	[19]
(4a)	2Cs(cr) + 2H_2O(l) = 2CsOH(sln) + H_2(g)	-404.56 ± 0.12	[49, 50]
(5a)	H_2(g)+ 1/2O_2(g) = H_2O(l)	-285.83 ± 0.04	[50]
(6a)	H_2O(l) + (sln) = H_2O(sln)	$\sim$0	[50, 53]
(7a)	2Cs(cr) + 2Mo(cr) + 7/2O_2(g) = α-$Cs_2Mo_2O_7$(cr)	-2301.6 ± 4.7	This work

^{a}The quoted uncertainty corresponds to the expanded uncertainty with a coverage factor of k=2.

4.2.2. $Cs_2Mo_3O_{10}$

Using a similar procedure for the determination of the standard enthalpy of formation of $Cs_2Mo_3O_{10}$, $Cs_2Mo_3O_{10}$ and MoO_3 were dissolved in 0.5009 mol·kg^{-1} and 0.5049 mol·kg^{-1} CsOH solutions, respectively. The dissolutions were again in all cases instantaneous. The corresponding thermochemical cycle is shown in Table 6, and the individual calorimetric results are listed in table 5.

Table 5: Calorimetric results for the dissolution of $Cs_2Mo_3O_{10}$ (M=713.660 g·mol^{-1}) in 0.5009^a mol·kg^{-1} CsOH solution, and MoO_3 (M=143.947 g·mol^{-1}) in 0.5049^a mol·kg^{-1} CsOH at 298.15 K. Solution calorimetry measurements were performed in (25.00 ± 0.03^b) mL solution at a pressure $p= (0.105 \pm 0.005^b)$ MPa, and in the temperature interval $T= (298.15 \pm 0.30^b)$ K

No.	$m(Cs_2Mo_3O_{10})^c$/mg	ΔT^d/mK	$C_p{}^e$/J·K^{-1}	Q^f/J	$\Delta_r H_m^o(298.15\ K)^g$/kJ·mol^{-1}
1	21.0	20.0	114.3	-2.3	-78.0
2	20.9	20.6	114.3	-2.4	-80.3
3	20.9	20.2	114.1	-2.3	-78.8
4	20.9	23.3	102.2	-2.4	-81.5
average					**-79.6 $\pm$ 3.2^e**
No.	$m(MoO_3)^c$/mg	ΔT^d/mK	$C_p{}^e$/J·K^{-1}	Q^f/J	$\Delta_r H_m^o(298.15\ K)^g$/kJ·mol^{-1}
1	12.6	61.0	110.5	-6.7	-77.1
2	12.8	60.0	111.9	-6.7	-75.5
3	12.6	61.1	110.6	-6.8	-77.2
4	12.6	60.4	111.0	-6.7	-76.6
average					**-76.6 $\pm$ 1.6^e**

m is the sample weight, ΔT the temperature change caused by the dissolution, C_p the energy equivalent of the calorimeter, Q the amount of heat generated by the dissolution, $\Delta_r H_m^o$(298.15 K) the corresponding molar enthalpy of reaction. ^{a}The expanded uncertainties (k=2) on the molalities are $U = 0.0002$ mol·kg^{-1}. ^{b}The quoted uncertainty corresponds to the standard uncertainty. ^{c}The expanded uncertainties (k=2) on the weights are $U(m) = 0.10$ mg. ^{d}The relative expanded uncertainties (k=2) on ΔT are $U_r(\Delta T) = 0.02$. ^{e}The relative expanded uncertainties (k=2) on C_p are $U_r(C_p) = 0.01$. ^{f}The relative expanded uncertainties (k=2) on Q are $U_r(Q) = 0.02$. ^{g}The expanded relative uncertainties (k=2) on $\Delta_r H_m^o$(298.15 K) are $U_r(\Delta_r H_m^o(298.15K)) = 0.02$. ^{e}Expanded uncertainty (k=2), corresponding to a 95% confidence interval.

Again, making sure that solutions (1b) and (2b) have the same composition, the enthalpy of the equilibrium reaction (4) is equal to $\Delta_r H_m^o = \Delta_r H_{2b} - \Delta_r H_{1b} = -(150.12 \pm 5.74)$ kJ·mol^{-1}.

$$3MoO_3(cr) + 2CsOH(sln) = Cs_2Mo_3O_{10}(cr) + H_2O(sln) \qquad (4)$$
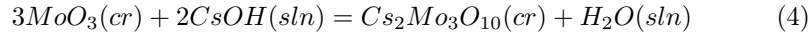
The molar enthalpy of dissolution of MoO_3(cr) in 0.5049 mol·kg^{-1} CsOH solution, i.e. $-(76.59 \pm 1.60)$ is in good agreement with the previous data in 0.1182 mol·kg^{-1} CsOH and the reported data in the literature as listed in the previous section [20, 26, 35]. There again the correction for the relative partial molar enthalpy of water in 0.5009 mol·kg^{-1} CsOH solution was considered negligible. Combining with the enthalpies of formation of H_2O(l) [50] and MoO_3(cr) [19], the standard enthalpy of formation of $Cs_2Mo_3O_{10}$ is derived as $\Delta_f H_m^o(Cs_2Mo_3O_{10},\ cr,\ 298.15\ K) = -(3075.6 \pm 6.5)$ kJ·mol^{-1}. Independently and in parallel to our study, the standard enthalpy of formation of $Cs_2Mo_3O_{10}$ was determined by Benigni and co-workers [35] using a CALSET calorimeter in 0.22608 mol·kg^{-1} CsOH solution on a sample prepared by solid state reaction of a (Cs_2MoO_4:2MoO_3) mixture. The value found in their work, i.e. $-(3077.17 \pm 3.47)$, is in excellent agreement with the present data for a sample prepared with a slightly different synthesis route (solid state reaction

13

of a ($Cs_2Mo_2O_7$:MoO_3) mixture) and with a dissolution in a slightly higher CsOH concentration. It is also interesting to point out that those two values are in good agreement with the optimized enthalpy of formation in the TAF-ID database ($-$ 3072.7 kJ·mol^{-1}).

Finally, considering here again that the uncertainty on the enthalpy of formation of MoO_3 is largely underestimated, and taking an uncertainty of 1% (i.e. $\pm$ 7.45 kJ·mol^{-1}) (see section 4.2.1), the derived value for the enthalpy of formation of $Cs_2Mo_3O_{10}$ becomes $-(3075.6 \pm 23.1)$ kJ·mol^{-1}.

Table 6: Thermochemical cycle used for the determination of the enthalpy of formation of $Cs_2Mo_3O_{10}$. Solution calorimetry measurements were performed at a pressure $p=$ (0.105 $\pm$ 0.005^a) MPa, and in the temperature interval $T=$ (298.15 $\pm$ 0.30^a) K. The enthalpy of formation of $Cs_2Mo_3O_{10}$ is derived with the relation: $\Delta_rH_{7b}=\Delta_rH_{1b}-\Delta_rH_{2b}+3\Delta_rH_{3b}+\Delta_rH_{4b}+\Delta_rH_{5b}-\Delta_rH_{6b}$.

	Reaction	$\Delta_r\mathbf{H_m^o(298.15\ K)/}$ $\mathbf{kJ\cdot mol^{-1}}$	Ref.
(1b)	$Cs_2Mo_3O_{10}(cr) + 430.55(CsOH\cdot111.204H_2O) = 3Cs_2MoO_4(sln) + 427.55CsOH(sln) + 47835.8272H_2O(sln)$	-79.6 ± 3.2^a	This work
(2b)	$3MoO_3(cr) + 433.55(CsOH\cdot110.3352H_2O) = 3Cs_2MoO_4(sln) + 427.55CsOH(sln) + 47835.8272H_2O(sln)$	-229.8 ± 4.8^a	This work
(3b)	$Mo(cr) + 3/2O_2(g) = MoO_3(cr)$	-745.0 ± 1.0	[19]
(4b)	$2Cs(cr) + 2H_2O(l) = 2CsOH(sln) + H_2(g)$	-404.56 ± 0.12	[49, 50]
(5b)	$H_2(g) + 1/2O_2(g) = H_2O(l)$	-285.83 ± 0.04	[50]
(6b)	$H_2O(l) + (sln) = H_2O(sln)$	~0	[50, 53]
(7b)	$2Cs(cr) + 3Mo(cr) + 5O_2(g) = Cs_2Mo_3O_{10}(cr)$	-3075.6 ± 6.5	This work

^{a}The quoted uncertainty corresponds to the expanded uncertainty with a coverage factor of $k=2$.

4.3. Phase diagram measurements in the Cs_2MoO_4-MoO_3 pseudo-binary section

The transition temperatures of $Cs_2Mo_2O_7$, $Cs_2Mo_3O_{10}$, $Cs_2Mo_5O_{16}$ and $Cs_2Mo_7O_{22}$ were measured in this work by TG-DSC and DSC. The obtained equilibrium data are listed in Table 7. The reliability of the applied temperature calibration was verified by measuring the three phase transitions and congruent melting temperature of Na_2MoO_4 (see Fig A.1 in Appendix). The obtained data were found in very good agreement with the recent review by Sugawara and Jin [56], which gave us good confidence on the applied temperature correction. No noticeable weight loss was observed as confirmed from the thermogravimetry results, hence no shift in composition is expected.

The derived transition temperature values are listed in Table 7 and shown on the Cs_2MoO_4-MoO_3 phase diagram computed using the TAF-ID thermodynamic database [34] (see Figure 2). Taken into account the combined standard deviation over successive runs and uncertainty associated with the temperature calibration procedure, the final uncertainty on the measured temperatures is estimated to be $\pm$ 5 K.

The measurements of the $Cs_2Mo_2O_7$ composition (Figure 3a) indicates a phase transition at $T_{tr}=$ (650 $\pm$ 5) K, slightly higher than the data reported previously in our group [21], i.e. (621.9 $\pm$ 5.0) K, and somewhat lower than the result of Hoekstra [30] ($\sim$668 K). The difference with the measurement

Table 7: Phase transition temperatures of the cesium molybdates collected by DSC at pressure (0.10 ± 0.01) MPa on the heating ramp using a 10 K·min^{-1} heating rate. Data collected with a 5 K·min^{-1} heating rate are indicated with an *. The corresponding compositions in the Cs_2O-MoO_3 pseudo-binary phase diagram is given by $x(MoO_3)$. The quoted uncertainties correspond to the standard uncertainties.

Composition	$x(MoO_3)^e$	T/K	Equilibrium	Equilibrium reaction	Ref.
Cs_2MoO_4	0.500	$839 \pm 5^{a,c}$	polymorphism	α-$Cs_2MoO_4 = \beta$-Cs_2MoO_4	This work
	0.500	$835 \pm 5^{b,c}$	polymorphism	α-$Cs_2MoO_4 = \beta$-Cs_2MoO_4	This work
	0.500	841.3 ± 1.0	polymorphism	α-$Cs_2MoO_4 = \beta$-Cs_2MoO_4	[19]
	0.500	844	polymorphism	α-$Cs_2MoO_4 = \beta$-Cs_2MoO_4	[30]
	0.500	$840.2 \pm 1.1^{b,c}$	polymorphism	α-$Cs_2MoO_4 = \beta$-Cs_2MoO_4	[21]
	0.500	841 ± 1	polymorphism	α-$Cs_2MoO_4 = \beta$-Cs_2MoO_4	[57]
	0.500	$1226 \pm 5^{a,c}$	congruent melting	β-$Cs_2MoO_4 = $ liq.	This work
	0.500	$1225 \pm 5^{b,c}$	congruent melting	β-$Cs_2MoO_4 = $ liq.	This work
	0.500	1229.5 ± 0.2	congruent melting	β-$Cs_2MoO_4 = $ liq.	[19]
	0.500	1213	congruent melting	β-$Cs_2MoO_4 = $ liq.	[30]
	0.500	1208.4 ± 0.5	congruent melting	β-$Cs_2MoO_4 = $ liq.	[21]
$Cs_2Mo_2O_7$	0.667	$650 \pm 5^{a,c}$	polymorphism	α-$Cs_2Mo_2O_7 = \beta$-$Cs_2Mo_2O_7$	This work
	0.667	$650 \pm 5^{b,c}$	polymorphism	α-$Cs_2Mo_2O_7 = \beta$-$Cs_2Mo_2O_7$	This work
	0.667	668	polymorphism	α-$Cs_2Mo_2O_7 = \beta$-$Cs_2Mo_2O_7$	[30]
	0.667	$725 \pm 5^{a,c}$	congruent melting	β-$Cs_2Mo_2O_7 = $ Liq.	This work
	0.667	$725 \pm 5^{b,c}$	congruent melting	β-$Cs_2Mo_2O_7 = $ Liq.	This work
	0.667	737	congruent melting	β-$Cs_2Mo_2O_7 = $ Liq.	[30]
	0.667	749	congruent melting	β-$Cs_2Mo_2O_7 = $ Liq.	[32]
	0.667	767	congruent melting	β-$Cs_2Mo_2O_7 = $ Liq.	[31]
	0.667	720 ± 1	congruent melting	β-$Cs_2Mo_2O_7 = $ Liq.	[21]
$Cs_2Mo_3O_{10}$	0.750	$806 \pm 5^{a,c}$	congruent melting	$Cs_2Mo_3O_{10} = $ Liq.	This work
	0.750	$806 \pm 5^{b,c}$	congruent melting	$Cs_2Mo_3O_{10} = $ Liq.	This work
	0.750	820	congruent melting	$Cs_2Mo_3O_{10} = $ Liq.	[30]
	0.750	823	congruent melting	$Cs_2Mo_3O_{10} = $ Liq.	[32]
	0.755	818	congruent melting	$Cs_2Mo_3O_{10} = $ Liq.	[31]
$Cs_2Mo_5O_{16}$	0.833	$781 \pm 5^{a,c}$	peritectoid	$Cs_2Mo_4O_{13} = Cs_2Mo_3O_{10} + Cs_2Mo_5O_{16}$	This work
	0.833	$783 \pm 5^{b,c,*}$	peritectoid	$Cs_2Mo_4O_{13} = Cs_2Mo_3O_{10} + Cs_2Mo_5O_{16}$	This work
	0.833	$813 \pm 5^{a,c}$	peritectic	$Cs_2Mo_5O_{16} = Cs_2Mo_7O_{22} + $ Liq.	This work
	0.833	$810 \pm 5^{b,c,*}$	peritectic	$Cs_2Mo_5O_{16} = Cs_2Mo_7O_{22} + $ Liq.	This work
	0.833	823	peritectic	$Cs_2Mo_5O_{16} = Cs_2Mo_7O_{22} + $ Liq.	[30, 31]
	0.813	818	peritectic	$Cs_2Mo_5O_{16} = Cs_2Mo_7O_{22} + $ Liq.	[32]
	0.833	$836 \pm 5^{a,d}$	liquidus	$Cs_2Mo_7O_{22} + $ Liq.' $ = $ Liq.	This work
	0.833	$825 \pm 5^{b,d,*}$	liquidus	$Cs_2Mo_7O_{22} + $ Liq.' $ = $ Liq.	This work
$Cs_2Mo_7O_{22}$	0.875	$812 \pm 5^{a,c}$	peritectic	$Cs_2Mo_5O_{16} = Cs_2Mo_7O_{22} + $ Liq.	This work
	0.875	$810 \pm 5^{b,c}$	peritectic	$Cs_2Mo_5O_{16} = Cs_2Mo_7O_{22} + $ Liq.	This work
	0.875	$836 \pm 5^{a,c}$	peritectic	$Cs_2Mo_7O_{22} = MoO_3 + $ Liq	This work
	0.875	$835 \pm 5^{b,c}$	peritectic	$Cs_2Mo_7O_{22} = MoO_3 + $ Liq	This work
	0.862	848	peritectic	$Cs_2Mo_7O_{22} = MoO_3 + $ Liq	[31]
	0.857	846	peritectic	$Cs_2Mo_7O_{22} = MoO_3 + $ Liq	[30]
	0.847	837	peritectic	$Cs_2Mo_7O_{22} = MoO_3 + $ Liq	[32]

[a]Data measured by TG-DSC.

[b]Data measured by DSC.

[c]Onset temperature of the heat flow signal.

[d]Peak maximum of the heat flow signal.

[e]Standard uncertainties u are $u(x(MoO_3))$=0.005.

reported in [21] is attributed to the different measurement configurations (open alumina crucible under oxygen flow in this work versus closed stainless steel crucible with nickel liner under argon in [21]). It is suspected that the magnetic transition of nickel ($\sim$ 627 K) was "masking" the phase transition in [21], as the energetics of the phase transition are very small. The present data are believed to be more reliable and are thus recommended. The polymorphic transition between the α phase stable at room temperature and the high temperature β phase corresponds to a transition between a monoclinic structure in space group $P2_1/c$ to an orthorhombic structure in space group $Pbcm$ [21]. The congruent melting temperature of β-$Cs_2Mo_2O_7$ was found at $T_{fus} = (725 \pm 5)$ K using the TG-DSC and DSC configurations, respectively. The latter data are in good agreement with the previously reported data in our research group (720.2 ± 5.0 K) [21], but lower than the data of Hoekstra [30] (737 K), Salmon and Caillet [32] (749 K), and Spitsyn and Kuleshov [31] (767 K). Note that in the CALPHAD model of the TAF-ID database, $Cs_2Mo_2O_7$ decomposes in a peritectic reaction at 736.5 K.

The melting temperature of $Cs_2Mo_3O_{10}$ (Figure 3b) is found at $T_{fus} = (806 \pm 5)$ K (TG-DSC and DSC), i.e. $\sim$15 K lower than the data of Hoekstra [30] (820 K), Salmon and Caillet [32] (823 K), and Spitsyn and Kuleshov [31] (818 K). Because the melting temperature is expected to be congruent at this composition, the onset temperature of the heat flow curve was selected herein. It is worth pointing out that the extremum temperature of the same heat flow signal yields (825 ± 5) K, which is closer to the literature data, and follows a logical trend compared to the neighbouring liquidus phase equilibria points (see Figure 2).

The peritectic decomposition of $Cs_2Mo_5O_{16}$ (Figure 3c) is detected at $T_{fus} = (813 \pm 5)$ K (TG-DSC), slightly lower than the data of Hoekstra, Spitsyn and Kuleshov (823 K) and Salmon and Caillet (818 K), and lower than calculated in the CALPHAD model of the TAF-ID database (818 K). In addition, a very small peak is collected at (781 ± 5) K, which is attributed to the peritectoid decomposition of $Cs_2Mo_4O_{13}$ impurity in the synthesized material (although the Bragg reflections of such phase were not observed on the X-ray diffraction pattern).

The peritectic decomposition of $Cs_2Mo_7O_{22}$ (Figure 3d) is found at $T_{fus} = (836 \pm 5)$ K (TG-DSC), again lower than the data of Hoekstra (846 K) and CALPHAD model of the TAF-ID database (856 K), but in good agreement with the data of Salmon and Caillet (837 K), although the latter data point was wrongly interpreted in their work as the polymorphic transition of a solid solution around the $Cs_2Mo_9O_{28}$ composition. Moreover, a small peak is detected at (812 ± 5) K, which is attributed to the peritectic decomposition of $Cs_2Mo_5O_{16}$ impurity in the synthesized material (again not observable by XRD).

Generally the collected data are found somewhat lower than Hoekstra [30]. Hoekstra reports that his DTA-TGA measurements were performed at a heating rate of 10 K/min, by taking the intercept between the extrapolated base line and the tangent to the slope of the peak. It is not completely clear from this description if a temperature correction was applied, and if the onset or off-

16

set intercept was selected, which could explain the slight discrepancy with our results.

Furthermore, transition temperatures of selected mixture compositions in the Cs_2MoO_4-MoO_3 pseudo-binary phase diagram were also measured using the TG-DSC set-up (see Figures B.2 and B.3). The obtained equilibrium data are listed in Table 8 and shown on the Cs_2MoO_4-MoO_3 phase diagram computed using the TAF-ID thermodynamic database [34] (Figure 2). The listed uncertainties in Table 8 ($\pm$ 10 K for the phase mixtures) correspond to the combined standard deviation over the successive cycles (typically over 3-4 cycles) and uncertainty associated with the temperature calibration procedure. No noticeable weight loss was observed as confirmed from the thermogravimetry results, hence no shift in composition is expected. The α to β phase transition in $Cs_2Mo_2O_7$ was also observed in the $Cs_2Mo_2O_7$-$Cs_2Mo_3O_{10}$ section, and the derived transition temperatures were found (within the $\pm$ 10 K uncertainty) in very good agreement with the data obtained for the pure $Cs_2Mo_2O_7$ sample, although the very small energetics of the phase transition resulted in a very small departure from the heat flow baseline curve.

Table 8: Equilibrium transition temperatures collected by DSC at pressure (0.10 $\pm$ 0.01) MPa on the heating ramp using a 10 K·min^{-1} heating rate. Data collected with a 5 K·min^{-1} heating rate are indicated with an *. The corresponding compositions in the Cs_2O-MoO_3 pseudo-binary phase diagram is given by $x(MoO_3)$. The quoted uncertainties correspond to the standard uncertainties.

Composition	$x(MoO_3)^e$	T/K	Equilibrium	Equilibrium reaction	Ref.
$(Cs_2Mo_2O_7$:$Cs_2Mo_3O_{10})$	0.706	$652 \pm 10^{a,c}$	polymorphism	α-$Cs_2Mo_2O_7 = \beta$-$Cs_2Mo_2O_7$	This work
$= (0.6$:$0.4)$	0.706	$719 \pm 10^{a,c}$	eutectic	β-$Cs_2Mo_2O_7 = Cs_2Mo_3O_{10}$ + Liq.	This work
	0.706	$787 \pm 10^{a,d}$	liquidus	$Cs_2Mo_3O_{10}$ + Liq.' = Liq.	This work
$(Cs_2Mo_2O_7$:$Cs_2Mo_3O_{10})$	0.730	$656 \pm 10^{a,c}$	polymorphism	α-$Cs_2Mo_2O_7 = \beta$-$Cs_2Mo_2O_7$	This work
$= (0.3$:$0.7)$	0.730	$715 \pm 10^{a,c}$	eutectic	β-$Cs_2Mo_2O_7 = Cs_2Mo_3O_{10}$ + Liq.	This work
	0.730	$812 \pm 10^{a,d}$	liquidus	$Cs_2Mo_3O_{10}$ + Liq.' = Liq.	This work
$(Cs_2Mo_3O_{10}$:$Cs_2Mo_5O_{16})$	0.773	$781 \pm 10^{a,c}$	peritectoid	$Cs_2Mo_4O_{13} = Cs_2Mo_3O_{10}$ + $Cs_2Mo_5O_{16}$	This work
$= (0.8$:$0.2)$	0.773	$816 \pm 10^{a,d}$	liquidus	$Cs_2Mo_3O_{10}$ + Liq.' = Liq.	This work
$(Cs_2Mo_3O_{10}$:$Cs_2Mo_5O_{16})$	0.811	$787 \pm 10^{a,c,*}$	peritectoid	$Cs_2Mo_4O_{13} = Cs_2Mo_3O_{10}$ + $Cs_2Mo_5O_{16}$	This work
$= (0.35$:$0.65)$	0.811	$812 \pm 10^{a,d,*}$	liquidus	$Cs_2Mo_5O_{16}$ + Liq.' = Liq.	This work

[a] Data measured by TG-DSC.

[b] Data measured by DSC.

[c] Onset temperature of the heat flow signal.

[d] Peak maximum of the heat flow signal.

[e] Standard uncertainties u are $u(x(MoO_3))$=0.005.

The measured eutectic equilibrium between $Cs_2Mo_2O_7$ and $Cs_2Mo_3O_{10}$ is found about 25 K lower than reported by Hoekstra [30] and about 15 K lower than calculated using the TAF-ID database [34]. The measured liquidus equilibria between $Cs_2Mo_2O_7$ and $Cs_2Mo_3O_{10}$ are also slightly lower than found by Hoekstra [30] and Spitsyn and Kuleshov [31]. By contrast, the measured temperature for the peritectoid decomposition of $Cs_2Mo_4O_{13}$ is in good agreement
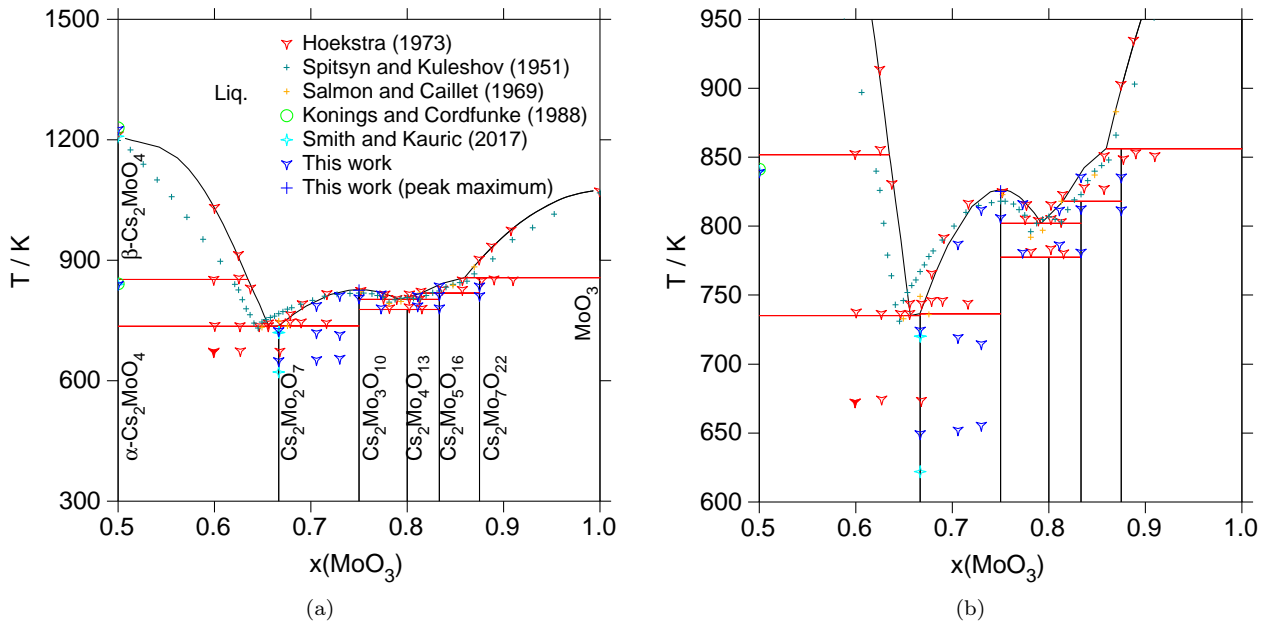
Figure 2: Pseudo-binary Cs_2MoO_4-MoO_3 section computed using the TAF-ID database [34] and comparison with the equilibrium data measured in this work, and reported in the literature by Spitsyn and Kuleshov [31], Salmon and Caillet [32], and Hoekstra [30].

with the data of Hoekstra [30], and the measured liquidus equilibria between $Cs_2Mo_3O_{10}$ and $Cs_2Mo_5O_{16}$ seem to follow reasonably well the predictions of the CALPHAD model and experimental data of [30] and [31]. The eutectic equilibrium could not be distinguished from the liquidus events on the heating ramp at those compositions due to the proximity of the equilibrium temperatures. Nevertheless, three events were detected on cooling, whose temperatures were not retained due to the occurrence of supercooling effects. When looking at Figure 2, it is clear that quite large discrepancies appear between the liquidus data of Hoekstra [30], Salmon and Caillet [32], and Spitsyn and Kuleshov [31], particularly in the Cs_2MoO_4-$Cs_2Mo_2O_7$ and $Cs_2Mo_7O_{22}$-MoO_3 pseudo-binary sections. Very little experimental details are reported in the paper by Spitsyn and Kuleshov [31] on their visual-polythermal technique, in particular the heating rate and cooling rates are unknown, and it is not clear if data were taken on heating or cooling (although the latter seems more probable considering the information given in their Table 3). The same is true for the paper of Salmon and Caillet [32]. The temperature calibration procedure of the DTA measurements is not specified. In view of these discrepancies and the observed differences with the measured data herein, it is clear that complementary measurements in selected regions of the phase diagram would be extremely valuable.

4.4. Transition enthalpy determinations

The enthalpies of congruent fusion of $Cs_2Mo_2O_7$ and $Cs_2Mo_3O_{10}$, and enthalpies associated with the peritectic decompositions of $Cs_2Mo_5O_{16}$ and $Cs_2Mo_7O_{22}$ were finally determined in this work by measuring the samples together with a reference material of well-known transition enthalpy. This configuration allows to calculate for each individual measurement cycle the detector sensitivity, which is assumed to remain the same at the temperatures of the transition events of the sample and reference. The references used for each individual measurement and their associated transition enthalpies are listed in Table 9. The reference materials were selected so that the transition temperatures of sample and reference materials were as close as possible without overlapping. Moreover, an oxide reference material was selected instead of a metal to ensure a comparable thermal properties of the two materials.

The well-known α-β phase transition of Cs_2MoO_4 (from an orthorhombic structure in space group $Pnma$ to a hexagonal structure in space group $P6_3/mmc$) was selected as reference for the measurement of $Cs_2Mo_2O_7$, with an associated transition enthalpy of (4.6 ± 0.1) kJ·mol^{-1}as recommended in the review of Cordfunke and Konings [19]. For $Cs_2Mo_3O_{10}$, sodium molybdate Na_2MoO_4 was chosen, which shows three polymorphic transitions before melting at (960 ± 3) K. The melting point of $Cs_2Mo_3O_{10}$ falls in between the α-β (from cubic $Fd\bar{3}m$ to orthorhombic structure of unknown space group) and β-γ (from orthorhombic to orthorhombic $Fddd$ structure) phase transitions of Na_2MoO_4 [56]. The first transition was selected for the analysis as it is much more energetic $(22.61 \pm 0.5$ kJ·mol$^{-1})$ that the second $(2.04 \pm 0.7$ kJ·mol$^{-1})$ [56]. Various studies have been reported on the high temperature heat capacity and enthalpy

19
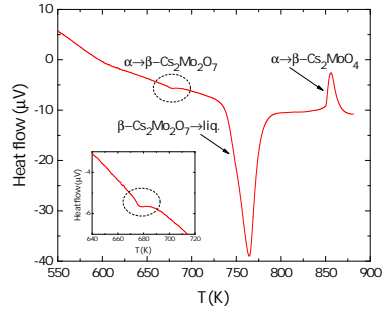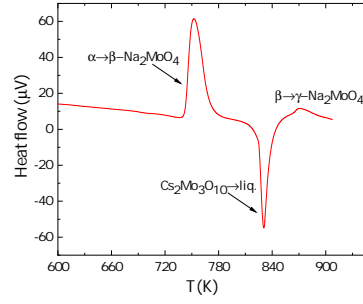
(a) $Cs_2Mo_2O_7$
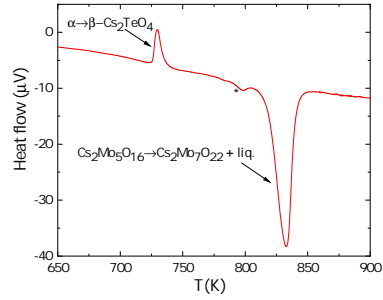
(b) $Cs_2Mo_3O_{10}$
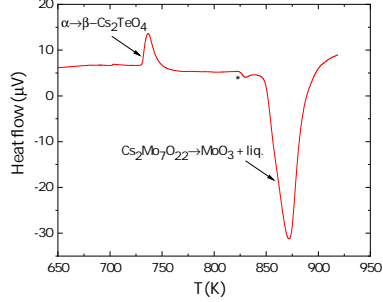
(c) $Cs_2Mo_5O_{16}$

(d) $Cs_2Mo_7O_{22}$

Figure 3: Heat flow curves versus temperature collected for (a) $Cs_2Mo_2O_7$, (b) $Cs_2Mo_3O_{10}$, (c) $Cs_2Mo_5O_{16}$ and (d) $Cs_2Mo_7O_{22}$. The events marked with * correspond in (c) to the peritectoid decomposition $Cs_2Mo_4O_{13} = Cs_2Mo_3O_{10} + Cs_2Mo_5O_{16}$; and in (d) to the peritectic $Cs_2Mo_5O_{16} = Cs_2Mo_7O_{22} + Liq.$

20

increment of Na_2MoO_4 [56, 58–63], but the results show quite some large discrepancies. The selected value for the α-β transition enthalpy is from the critical analysis of past studies and newly measured DSC and drop calorimetry measurements by Sugawara and Jin [56], which are generally in good agreement with the average value of the previous studies. Finally, the existence of a α-β phase transition in cesium tellurate Cs_2TeO_4 (from an orthorhombic structure in space group $Pnma$ to a hexagonal structure in space group $P6_3/mmc$) was recently revealed in our research group, and the associated transition enthalpy determined as (2.67 ± 0.14) kJ·mol^{-1}[36]. The latter data were used to assess the enthalpies of the peritectic decompositions in $Cs_2Mo_5O_{16}$ and $Cs_2Mo_7O_{22}$.

Table 9: Transition temperatures and transition enthalpies of the selected reference materials.

Sample	Transition sample	Reference	Transition reference	$T_{tr}(ref)$/K	$\Delta_{tr}H_m^o$(ref)/ (kJ·mol^{-1})	Ref.
$Cs_2Mo_2O_7$	Polymorphism/Congruent melting	Cs_2MoO_4	α-$Cs_2MoO_4 = \beta$-Cs_2MoO_4	(841 ± 1)	(4.6 ± 0.1)	[19]
$Cs_2Mo_3O_{10}$	Congruent melting	Na_2MoO_4	α-$Na_2MoO_4 = \beta$-Na_2MoO_4	(728 ± 4)	(22.61 ± 0.50)	[56]
$Cs_2Mo_5O_{16}$	Peritectic	Cs_2TeO_4	α-$Cs_2TeO_4 = \beta$-Cs_2TeO_4	(712 ± 5)	(2.67 ± 0.14)	[36]
$Cs_2Mo_7O_{22}$	Peritectic	Cs_2TeO_4	α-$Cs_2TeO_4 = \beta$-Cs_2TeO_4	(712 ± 5)	(2.67 ± 0.14)	[36]

The heat flow curves for each composition are shown in Figures 3. Note that the opposite directions for the sample and reference (endothermic) events is due to the different positioning in the reference and sample crucibles, respectively. Multiple measurements were performed (Table 10) and averaged, yielding for the congruent melting transitions of β-$Cs_2Mo_2O_7$ and $Cs_2Mo_3O_{10}$: $\Delta_{fus}H_m^o(\beta$-$Cs_2Mo_2O_7$, cr, $T_{fus}) = (81.2 \pm 7.1)$ kJ·mol^{-1}and $\Delta_{fus}H_m^o(Cs_2Mo_3O_{10}$, cr, $T_{fus}) = (81.8 \pm 16.8)$ kJ·mol^{-1}, respectively. In the case of $Cs_2Mo_5O_{16}$ and $Cs_2Mo_7O_{22}$, the transitions measured correspond to two peritectic decompositions with an associated enthalpy equal to: $\Delta_{tr}H_m^o(Cs_2Mo_5O_{16}$, cr, $T_{peritectic})$ = (121.3 ± 8.2) kJ·mol^{-1}and $\Delta_{tr}H_m^o(Cs_2Mo_7O_{22}$, cr, $T_{peritectic}) = (216.5 \pm 24.2)$ kJ·mol^{-1}, respectively. The reported uncertainties are expanded uncertainties with a coverage factor $(k = 2)$, that include the error associated with the uncertainty on the transition enthalpy of the reference material, and the error associated with the choice of the baseline for the peak integration (spline, linear or tangential sigmoid). It should be noted that, in the present analysis, no corrections were applied for the presence of small impurities in the batch of $Cs_2Mo_5O_{16}$ and $Cs_2Mo_7O_{22}$ (of $Cs_2Mo_4O_{13}$ and $Cs_2Mo_5O_{16}$, respectively) as suggested by the DSC measurements and indicated with an asterisk * in Figure 3. However, this means that the uncertainties on the results should be increased slightly. In addition, the same procedure was applied for the determination of the transition enthalpy of the polymorphic transition in $Cs_2Mo_2O_7$, yielding $\Delta_{tr}H_m^o(Cs_2Mo_2O_7$, cr, $T_{tr}) = (423 \pm 191)$ J·mol^{-1}. The small transition enthalpy is related to the fact that the α and β forms have closely related structures [21]. The value derived herein is subject to a large uncertainty because of the small energetics. We hence recommend to repeat the measurements with much larger batches to confirm the present result. Nevertheless, the mea-

sured data can serve as first input for the development of a thermodynamic model for the Cs-Mo-O system using the CALPHAD methodology.

Table 10: Transition enthalpy data collected by DSC at pressure (0.10 ± 0.01) MPa. Data collected with a 5 K·min^{-1} heating rate are indicated with an *. The quoted uncertainties correspond to expanded uncertainties U with a coverage factor $k = 2$, corresponding to a 95% confidence interval. They do not include systematic uncertainties.

m(sample)/ (mg)	m(ref)/ (mg)	$\Delta_{tr}H_{\mathbf{m}}^{\mathbf{o}}(\mathbf{ref})$/ (kJ·mol^{-1})	A_{ref}/ (μV·s)	s_{ref}/ (μV·mW^{-1})	A_{sample}/ (μV·s)	$\Delta_{tr}H_{\mathbf{m}}^{\mathbf{o}}(\mathbf{sample})$/ (kJ·mol^{-1})
$Cs_2Mo_2O_7$ (congruent melting) versus Cs_2MoO_4 reference						
62.16	98.85	4.6 ± 0.1	416.43	0.3899	3504.92	82.38 ± 13.43
45.46	102.47	4.6 ± 0.1	449.74	0.4062	2673.52	82.48 ± 12.41
46.91	103.99	4.6 ± 0.1	441.71	0.3931	2565.52	79.25 ± 11.44
Average						$(\mathbf{81.2 \pm 7.1}^a)$
$Cs_2Mo_2O_7$ (α-β phase transition) versus Cs_2MoO_4 reference						
62.16	98.85	4.6 ± 0.1	416.43	0.3899	17.75	0.4172 ± 0.3639
45.46	102.47	4.6 ± 0.1	449.74	0.4062	15.19	0.4686 ± 0.3577
46.91	103.99	4.6 ± 0.1	441.71	0.3931	12.87	0.3977 ± 0.2887
Average						$(\mathbf{0.423 \pm 0.191}^a)$
$Cs_2Mo_3O_{10}$ (congruent melting) versus Na_2MoO_4 reference						
56.9	80.22	22.61 ± 0.50	5276.72	0.5991	3918.13	82.03 ± 22.25
58.96	87.69	22.61 ± 0.50	5731.48	0.5953	3985.22	81.03 ± 39.23
90.01	122.31	22.61 ± 0.50	8031.95	0.5981	6180.77	81.94 ± 33.91
Average						$(\mathbf{81.8 \pm 16.8}^{a,b})$
$Cs_2Mo_5O_{16}$ (peritectic) versus Cs_2TeO_4 reference						
55.36	113.16	2.67 ± 0.14	451.40*	0.6834	4598.55*	121.74 ± 9.58
40.9	113.78	2.67 ± 0.14	439.1*	0.6611	3242.19*	120.09 ± 16.01
Average						$(\mathbf{121.3 \pm 8.2}^a)$
$Cs_2Mo_7O_{22}$ (peritectic) versus Cs_2TeO_4 reference						
49.34	111.11	2.67 ± 0.14	398.72	0.6148	5158.21	219.28 ± 35.16
45.77	109.08	2.67 ± 0.14	388.53	0.6102	4633.16	213.91 ± 33.32
Average						$(\mathbf{216.5 \pm 24.2}^a)$

[a] The final averaged result X was calculated as a weighted mean using the formula $X = \sum_i(X_i/\sigma_i^2)/\sum_i(1/\sigma_i^2)$, while the uncertainty was calculated using the formula $\sigma_X = \sqrt{\frac{1}{\sum_i(1/\sigma_i^2)}}$ as recommended in [64] considering that the individual measurements are independent source of data since fresh materials and crucibles were used each time.
[b] The rather large uncertainty on the data for $Cs_2Mo_3O_{10}$ originates mostly from the choice of the baseline, which is affected by a slight overlap between the fusion event of the sample and second transition of the reference Na_2MoO_4 material.

5. Conclusions

Experimental studies in the Cs_2MoO_4-MoO_3 phase diagram are reported in this work, that can serve as input for the thermodynamic assessment of the

Cs-Mo-O system using the CALPHAD methodology, and *in fine* for thermodynamic modelling purposes of the fission products chemistry in Light Water Reactors and next generation Sodium-cooled Fast Reactors and Lead-cooled Fast Reactors and assessment of the source term under accidental conditions. The enthalpies of formation of α-$Cs_2Mo_2O_7$ and $Cs_2Mo_3O_{10}$ have been determined in 0.1002 mol·kg^{-1} and 0.5009 mol·kg^{-1} CsOH solutions, respectively. The values derived herein, $\Delta_f H_m^o(\alpha$-$Cs_2Mo_2O_7$, cr, 298.15 K$) = -(2301.6 \pm 4.7)$ kJ·mol^{-1} and $\Delta_f H_m^o(Cs_2Mo_3O_{10}$, cr, 298.15 K$) = -(3075.6 \pm 6.5)$ kJ·mol^{-1}, respectively, are in very good agreement with the previous study of O'Hare and Hoekstra [23] and the recently reported data by Benigni et al. [35]. In addition, phase equilibria measurements in this system are reported, which are found generally slightly lower than the previous studies by Hoekstra [30] and Spitsyn and Kuleshov [31] in the 1970s and 1950s. The reliability of the applied temperature calibration was confirmed with the measurement of the well-known transitions in Na_2MoO_4, which gives us confidence on the newly reported data. Finally, the enthalpies of fusion of β-$Cs_2Mo_2O_7$ and $Cs_2Mo_3O_{10}$ and of peritectic decompositions of $Cs_2Mo_5O_{16}$ and $Cs_2Mo_7O_{22}$ have been determined for the first time using differential scanning calorimetry and an internal standard reference. Obtaining reliable experimental data for the multi-element fission products systems in LWRs and fast neutron reactors is key for the prediction of the formed phases in the irradiated fuel as a function of temperature, burnup and thus oxygen potential conditions, and for the development of simulation tools that can predict the fuel behaviour under any operating and accidental conditions.

6. Acknowledgements

References

[1] J. Rest and A. W. Cronenberg. J. Nucl. Mater. 150 (1987) 203–225.

[2] H. Kleykamp. J. Nucl. Mater. 131 (1985) 221–246.

[3] G. Brillant. J. Nucl. Mater. 397 (2010) 40–47.

[4] Y. Guerin. Comprehensive Nuclear Materials, Chapter 2.21: Fuel performance of Fast Spectrum Oxide Fuel, Elsevier, (2012).

[5] M. Tourasse, M. Boidron, and B. Pasquet. J. Nucl. Mater. 1800 (1992) 49–57.

[6] J.-C. Dumas. *Etude des conditions de formation du Joint-Oxyde-Gaine dans les combustibles oxydes mixtes des reacteurs à neutrons rapides, observations et proposition d'un modèle de comportement des produits de fission volatils.* PhD thesis, Institut national polytechnique de Grenoble, Grenoble, France, (1995).

[7] K. Maeda and T. Asaga. J. Nucl. Mater. 327 (2004) 1–10.

[8] Tam Ngoc Pham Thi. *Caractérisation et modélisation du comportement thermodynamique du combustible RNR-Na sous irradiation.* PhD thesis, Ecole Doctorale Physique et Sciences de la Matière (Aix-Marseille University), (2014).

[9] R. Parrish, A. Winston, J. Harp, and A. Aitkaliyeva. J. Nucl. Mater. 527 (2019) 151794.

[10] K. Samuelsson, J.-C. Dumas, B. Sundman, J. Lamontagne, and C. Gu'eneau. J. Nucl. Mater. 532 (2020) 151969.

[11] F. Cappia, B. D. Miller, J. A. Aguiar, L. He, D. J. Murray, B. J. Frickey, J. D. Stanek, and J. M. Harp. J. Nucl. Mater. 531 (2020) 151964.

[12] R. J. M. Konings and E. H. P. Cordfunke. Thermochim. Acta 124 (1988) 157–162.

[13] G. Wallez, P. E. Raison, A. L. Smith, N. Clavier, and N. Dacheux. J. Solid State Chem. 215 (2014) 225–230.

[14] T. Ishii and T. Mizuno. J. Nucl. Mater. 231 (1996) 242–244.

[15] K. Minato, M. Takano, K. Fukuda, S. Sato, and H. Ohashi. J. Nucl. Mater. 255 (1997) 18–23.

[16] I. Johnson. J. Phys. Chem. 79 (1975) 722–726.

[17] O. Fabrichnaya. *Cesium-Molybdenum-Oxygen. In: Ternary Alloy Systems: Phase diagrams, Crystallographic and Thermodynamic Data critically evaluaed by MSIT. Subvol. C. Non-ferrous metal systems. Pt. 4: Selected nuclear materails and engineering systems.* Springer-Verlag, (2007).

[18] P. Villars and K. Cenzual. ASM International, Materials Park, Ohio, USA, Technical report, (2018/2019).

[19] E. H. P. Cordfunke and R. J. M. Konings. Thermochemical data for reactor materials and fission products, Elsevier Science Publishers B. V., (1990).

[20] P. A. G O'Hare and H. R. Hoekstra. J. Chem. Thermodynamics 5 (1973) 851–856.

[21] A. L. Smith, G. Kauric, L. van Eijck, K. Goubitz, G. Wallez, J.-C. Griveau, E. Colineau, N. Clavier, and R. J. M. Konings. J. Solid State Chem. 253 (2017) 89–102.

[22] D. W. Osborne, H. E. Flotow, and H. R. Hoekstra. J. Chem. Thermodynamics 6 (1974) 179–183.

[23] P. A. G O'Hare and H. R. Hoekstra. J. Chem. Thermodynamics 7 (1975) 279–284.

[24] R. Kohli. Thermochim. Acta 237 (1994) 241–245.

[25] T.-M.-D. Do, S. Sujatanond, and T. Ogawa. Journal of Nuclear Science and Technology 55 (2018) 348–355.

[26] A.L. Smith, M.-C. Pignié, L. van Eijck, J.-C. Griveau, E. Colineau, and R.J.M. Konings. J. Chem. Thermodynamics 120 (2018) 205–216.

[27] D. R. Fredrickson and M. G. Chasanov. Anal. Calorimetry (1974) 723–730.

[28] L. Denielou, J. P. Petitet, and C. Tequi. J. Chem. Thermodynamics 7 (1975) 901–902.

[29] R. Kohli and W. Lacom. Thermochim. Acta 57 (1982) 155–160.

[30] H. R. Hoekstra. Inorg. Nucl. Chem. Letters 9 (1973) 1291–1301.

[31] V. I. Spitsyn and I. M. Kuleshov. J. Gen. Chem. USSR 21 (1951) 1493.

[32] R. Salmon and P. Caillet. Bull. Soc. Chim. Fr. 5 (1969) 1569–1573.

[33] Zh. G. Bazarova, K. N. Fedorov, M. V. Mokhosoev, R. P. Shulunov, G. D. Tsyrenova, and L. N. Korsun. Russ. J. Inorg. Chem. 35 (1990) 1505–1508.

[34] Thermodynamics of Advanced Fuels-International Database (TAF-ID), www.oecd-nea.org/science/taf-id/, OECD, NEA, Technical report.

[35] P. Benigni, G. Mikaelian, E. Ruiz, C. Perrin-Pellegrino, and J. Rogez. J. Chem. Eng. Data 65(8) (2020) 3875–3883.

[36] E. Epifano, A. Volfi, M. Abbink, H. Nieuwland, L. van Eijck, G. Wallez, D. Banerjee, P. M. Martin, and A. L. Smith. Inorganic Chemistry 59(14) (2020) 10172–10184.

[37] J. Rodriguez-Carvajal. Physica B 192 (1993) 55–69.

[38] G. A. Uriano. National Bureau of Standards, Technical report, (1981).

[39] V. B. Parker. Nat. Stand. Ref. Data Ser., Nat. Bur. Stand. (U.S.) 2, Technical report, (1965).

[40] I. Wadsö and R. N. Goldberg. Pure Appl. Chem. 73 (2001) 1625–1639.

[41] D. D. Wagman, W. H. Evans, V. B. Parker, R. H. Schumm, I. Halow, S. M. Bailey, K. L. Churney, and R. L. Nuttall. J. Phys. Chem. Ref. Data 11 (1982).

[42] R. L. Graham and L. Hepler. J. Am. Chem. Soc. 78 (1956) 4846.

[43] M. F. Koehler, L. B. Pankratz, and R. Barany, Sodium molybdates, heats of formation. US Bureau of Mines, (1962).

[44] R. P. Tangri, V. Venugopal, and D. K. Bose. Thermochim. Acta 198 (1992) 259–265.

[45] B. N. Taylor and C. E. Kuyatt. NIST National Institute of Standards and Technology, Technical Report 1297, (1994).

[46] G. W. H. Höhne, H. K. Cammenga, W. Eysel, E. Gmelin, and W. Hemminger. Thermochimica Acta 160 (1990) 1–12.

[47] R. Enjalbert, F. Guinneton, and J. Galy. Acta Crystallogr. C 55 (1999) 273–276.

[48] B. M. Gatehouse and B. K. Miskin. Acta Crystallogr. B 31 (1975) 1293–1299.

[49] S. R. Gunn. The Journal of Physical Chemistry 71(5) (1967) 1386–1390.

[50] J. D. Cox, D. D. Wagman, and V. A. Medvedev. Hemisphere Publishing Corp., (1998).

[51] L. V. Gurvich, G. A. Bergman, L. N. Gorokhov, V. S. Iorish, V. Ya. Leonidov, and V. S. Yungman. J. Phys. Chem. Ref. Data 26 (1997) 1031–1110.

[52] R. J. M. Konings, E. H. P. Cordfunke, and W. Ouweltjes. J. Chem. Thermodynamics 20 (1988) 777–780.

[53] D. D. Wagman, W. H. Evans, V. B. Parker, R. H. Schumm, I. Halow, S. M. Balley, K. L. Churney, and R. L. Nuttal. American Chemical Society and the American Institute of Physics for the National Bureau of Standards, (1982).

[54] B. A. Staskiewicz, J. R. Tucker, and P. E. Snyder. Journal of the American Chemical Society 77(11) (1955) 2987–2989.

[55] A. D. Mah. J. Phys. Chem. 61(11) (1957) 1572–1573.

[56] T. Sugawara and K. Jin. Thermochim. Acta 669 (2018) 185–193.

[57] Z. A. Solodovnikova, S. F. Solodovnikov, and E. S.Zolotova. Acta Crystallogr. C 62 (2006) 16–18.

[58] L. Denielou, Y. Fournier, J.-P. Petitet, and Ch. Tequi. C. R. Acad. Sci. 272 (1971) 1855–1857.

[59] A. P. Zhidikova and O. L. Kuskov. Geochem. Int. 8 (1972) 722–724.

[60] V. S. Iyer, R. Agarwal, K. N. Roy, S. Venkateswaran, V. Venugopal, and D. D. Sood. J. Chem. Thermodyn. 22 (1990) 439–448.

[61] V. P. Glushko. VINITI, Moscow, (1981).

[62] R. Riccardi and C. Sinistri. Ric. Sci. Rend. Sez. A 8(5) (1965) 1026.

[63] A. V. Khoroshilov, G. A. Sharpataya, K. S. Gavrichev, and M. A. Ryumin. Russ. J. Inorg. Chem. 57(8) (2012) 1123–1127.

[64] R. Guillaumont, T. Fanghänel, J. Fuger, I. Grenthe, V. Neck, D. A. Palmer, and M. H. Rand. Update on the chemical thermodynamics of uranium, neptunium, plutonium, americium & technetium, OECD Nuclear Energy Agency, Data Bank, (2003).

[65] P. Caillet. Bulletin de la Société chimique de France 12 (1967) 4750–4755.

Appendices

A. Calorimetry data Na_2MoO_4

To assess the reliability of the temperature calibration of the TG-DSC and DSC measurements, the well-known phase transitions of Na_2MoO_4 were collected in this work using the same set-up as for the measurements in the Cs_2MoO_4-MoO_3 pseudo-binary section. The collected data are shown in Fig. A.1 (TG-DSC) and listed in Table A.1 (TG-DSC and DSC). The agreement with the review by Sugawara and Jin [56] is very good, with deviations below 1.7 K for the TG-DSC set-up and below 4 K for the DSC set-up, except for the β-γ transition, where the difference is ~10 K. It should be noted, however, that the latter transition is the least energetic which makes the temperature determination less accurate, and that the data reported in the literature spread over the range (853 ± 2) K [65] to (866 ± 3) K [58].

Table A.1: Equilibrium data collected in this work by TG-DSC and DSC at pressure (0.10 ± 0.01) MPa on Na_2MoO_4. The quoted uncertainties correspond to the standard uncertainties.

Transition	T/K (TG-DSC)	T/K (DSC)	T/K [56]
α-$Na_2MoO_4 = \beta$-Na_2MoO_4	(726 ± 5)	(725 ± 5)	(728 ± 4)
β-$Na_2MoO_4 = \gamma$-Na_2MoO_4	(852 ± 5)	(850 ± 5)	(861 ± 4)
γ-$Na_2MoO_4 = \delta$-Na_2MoO_4	(913 ± 5)	(911 ± 5)	(914 ± 2)
δ-Na_2MoO_4 = Liq.	(959 ± 5)	(956 ± 5)	(960 ± 3)

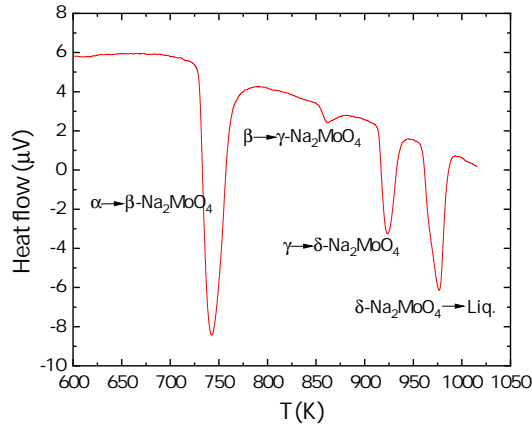Figure A.1: Heat flow curves versus temperature collected for Na_2MoO_4 by TG-DSC.

B. Calorimetry data in the Cs_2MoO_4-MoO_3 pseudo-binary section

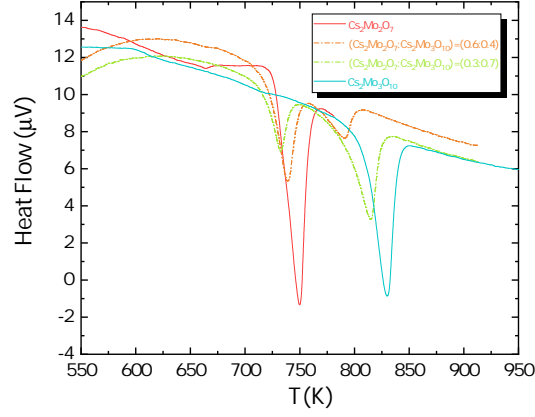Figure B.2: Heat flow curves versus temperature collected in the $Cs_2Mo_2O_7$-$Cs_2Mo_3O_{10}$ pseudo-binary section by TG-DSC.
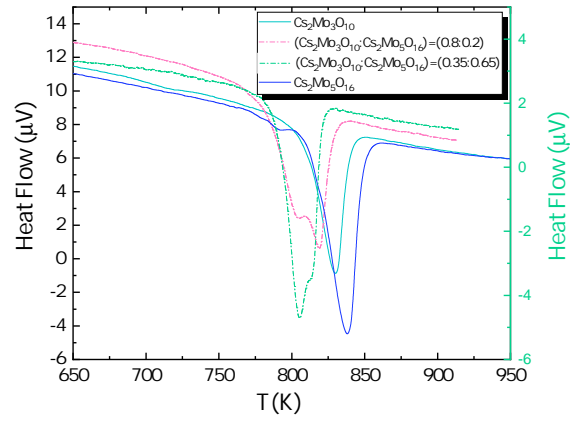
Figure B.3: Heat flow curves versus temperature collected in the $Cs_2Mo_3O_{10}$-$Cs_2Mo_5O_{16}$ pseudo-binary section by TG-DSC.

C. DSC data treatment
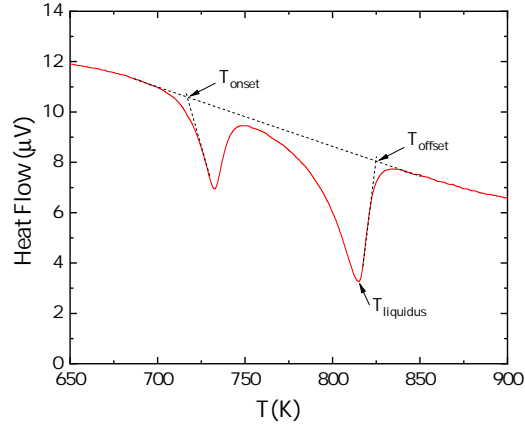
Figure C.4: Representative example of a DSC heat flow signal on the heating ramp, showing the onset temperature T_{onset}, the offset temperature T_{offset} and the peak extremum of the last thermal event taken as the liquidus temperature. The data treatment is exemplified on the $(Cs_2Mo_2O_7:Cs_2Mo_3O_{10})=(0.3:0.7)$ mixture.

D. Rietveld refinements

Table D.2: Refined atomic positions in α-$Cs_2Mo_2O_7$ derived from the X-ray diffraction refinement. $R_{wp} = 32.3$, $R_{exp} = 8.43$, $\chi^2 = 14.7$. Background: Linear interpolation between operator-selected points in the pattern with refinable heights.

Atom	Ox. State	Wyckoff	x	y	z	$B_0(\text{Å}^2)$
Cs1	+1	4e	0.3069(5)	0.4815(7)	0.702(1)	1.4(2)*
Cs2	+1	4e	0.1695(5)	0.5130(7)	0.219(1)	0.8(1)*
Cs3	+1	4e	0.0521(6)	0.3215(7)	0.708(1)	1.2(2)*
Cs4	+1	4e	0.5412(6)	0.3243(7)	0.784(1)	1.0(2)*
Mo1	+6	4e	0.2859(9)	0.252(1)	0.482(2)	0.34(1)*
Mo2	+6	4e	0.4199(8)	0.4035(8)	0.248(2)	0.8(1)*
Mo3	+6	4e	0.2222(9)	0.754(1)	0.508(2)	0.6(1)*
Mo4	+6	4e	0.0778(8)	0.6058(8)	0.776(2)	0.5(1)*
O1	-2	4e	0.2104(8)*	0.1786(7)*	0.525(2)*	0.6(1)*
O2	-2	4e	0.2270(8)*	0.3449(8)*	0.443(2)*	0.9(2)*
O3	-2	4e	0.3134(8)*	0.2130(7)*	0.237(2)*	0.8(1)*
O4	-2	4e	0.3814(7)*	0.1486(8)*	0.551(1)*	0.4(1)*
O5	-2	4e	0.4240(7)*	0.3297(8)*	0.444(2) *	0.6(2)*
O6	-2	4e	0.5269(7)*	0.4395(7)*	0.222(2)*	0.6(2)*
O7	-2	4e	0.3641(6)*	0.4955(7)*	0.281(2)*	0.3(1)*
O8	-2	4e	0.3225(7)*	0.6919(7)*	0.548(2)*	0.4(1)*
O9	-2	4e	0.2719(9)*	0.8597(7)*	0.458(2)*	1.1(2)*
O10	-2	4e	0.1977(7)*	0.7778(7)*	0.758(2)*	0.3(1)*
O11	-2	4e	0.1440(8)*	0.6369(8)*	0.569(1)*	0.3(1)*
O12	-2	4e	0.0864(8)*	0.8216(9)*	0.457(2) *	0.8(2)*
O13	-2	4e	-0.0292(9)*	0.6116(8)*	0.690(2) *	1.1(2)*
O14	-2	4e	0.1003(7)*	0.4918(7)*	0.828(1)*	0.4(2)*

*The thermal agitation factors and atomic positions of the oxygen atoms were not refined, but taken

from the neutron diffraction data of [21].

Table D.3: Refined atomic positions in $Cs_2Mo_3O_{10}$ derived from the X-ray diffraction refinement. $R_{wp} = 14.9$, $R_{exp} = 4.27$, $\chi^2 = 12.1$. Background: Linear interpolation between operator-selected points in the pattern with refinable heights.

Atom	Ox. State	Wyckoff	x	y	z	$B_0(Å^2)$
Cs	+1	8f	0.17802(9)	0.4205(2)	0.1592(2)	0.64(4)
Mo1	+6	8f	1/2	0.2260(3)	1/4	0.47(4)
Mo2	+6	8f	0.3934(1)	0.4264(3)	0.4759(2)	0.47(4)
O1	-2	8f	0.4703(9)	0.120(2)	0.098(1)	2.0(2)
O2	-2	8f	0.3916(9)	0.329(2)	0.335(2)	2.0(2)
O3	-2	8f	0.5136(8)	0.410(2)	0.398(1)	2.0(2)
O4	-2	8f	0.3801(9)	0.336(1)	0.641(2)	2.0(2)
O5	-2	8f	0.2953(8)	0.553(2)	0.402(1)	2.0(2)

Table D.4: Refined atomic positions in $Cs_2Mo_5O_{16}$ derived from the X-ray diffraction refinement. $R_{wp} = 21.4$, $R_{exp} = 4.81$, $\chi^2 = 19.8$. Background: Linear interpolation between operator-selected points in the pattern with refinable heights.

Atom	Ox. State	Wyckoff	x	y	z	$B_0(Å^2)$
Cs	+1	8f	0.2225(1)	0.1655(4)	0.3407(2)	0.92(5)
Mo1	+6	4e	0	0.1397(9)	1/4	0.49(4)
Mo2	+6	8f	0.1109(2)	0.7870(6)	0.4651(3)	0.49(4)
Mo3	+6	8f	0.0624(2)	0.3326(7)	0.6109(3)	0.49(4)
O1	-2	8f	0.102(1)	0.072(3)	0.391(2)	0.08(16)
O2	-2	8f	0.072(1)	0.081(4)	0.536(2)	0.08(16)
O3	-2	8f	0.019(1)	0.140(4)	0.672(2)	0.08(16)
O4	-2	8f	0.114(1)	0.591(4)	0.376(2)	0.08(16)
O5	-2	8f	0.075(1)	0.624(4)	0.538(2)	0.08(16)
O6	-2	8f	0.015(1)	0.7178(3)	0.669(2)	0.08(16)
O7	-2	8f	0.2208(9)	0.853(4)	0.713(1)	0.08(16)
O8	-2	8f	0.151(1)	0.358(4)	0.755(2)	0.08(16)